1st Solicitation for Single Investigator Research Grants (AFC113)

ALPHA FOUNDATION FOR THE IMPROVEMENT OF MINE SAFETY AND HEALTH

Final Technical Report

1.0 Cover Page

Project Title: Numerical Modeling Methodologies for Assessing Burst Potential in Coal Mines

Grant Number: AFC113-02

Organization: Colorado School of Mines
Department of Mining Engineering

Principal Investigator: Prof. Ugur Ozbay

Contact Information: Email: mozbay@mines.edu
Phone: 303-273 3123

Period of Performance: November 1, 2013 –October 31, 2015

Acknowledgment/Disclosure

This study was sponsored by the Alpha Foundation for the Improvement of Mine Safety and Health, Inc. (ALPHA FOUNDATION). The views, opinions and recommendations expressed herein are solely those of the authors and do not imply any endorsement by the ALPHA FOUNDATION, its Directors and staff.

Contents

2.0 Executive Summary

The objective of this research is to develop and apply numerical modeling methodologies for investigating energy released during quasi-brittle failure of highly stressed rock in underground mines. This objective was accomplished by constructing numerical models of past incidents of rock burst, coal bump, and massive collapse. Each case was modeled from well-established estimates of the material properties and *in situ* conditions which led to the failures. The dynamic energy released in the models was then compared to the magnitude of failure seen in the true mining case. Several models were constructed of one coal mine and one trona mine. The energy released due to instability was calculated through static and dynamic energy balances, both of which demonstrated that the energy-based measure of instability provides a direct assessment of unstable failure conditions as they emerge within simulated mine layouts.

Isolated single pillar models were developed and tested using variations in strength and post-failure material behaviors. Two- and three-dimensional full-scale mine models were then developed by installing *in situ* stress conditions and progressively mining material from the simulated coal and trona seams.

Back-analysis studies of the Crandall Canyon coal mine collapse provided an opportunity to assess the effects of various material and coal/rock interface properties on unstable failure. Results of these studies reveal that the failure of quasi-brittle coal material, combined with a coal/rock interface capable of shear slip, facilitates sudden dynamic failure within coal pillars with squat geometries and large width-to-height ratios. A drop in shear strength during slip of the interface was seen to dramatically increase the energy released during a simulated collapse event. Future analyses of coal pillar strength and failure behavior may benefit from the combined use of softening parameters for material in compression and for bedding plane discontinuities in shear.

The energy calculation methods developed in this study were extended to several collapse events experienced at the General Chemical trona mine. Complex behavior was introduced for the overburden strata and a range of support characteristics were applied to a simulated room-and-pillar layout in retreat. The excess energy calculated in this case was observed to increase with the width of the span and was reduced when pillars were assumed to have a more ductile response. The behavior of the model corresponded well with observations made in the mine.

The studies presented in this report uncover rational mechanisms for dynamic failures of squat coal pillars in coal mines and the combined failure of overburden strata and slender retreat pillars in a trona mine. The excess energy increases significantly as brittleness of the mine pillars is increased. Several combinations of material properties within the models led to excess energy values which were comparable to the radiated seismic energy calculated from the seismic record of each event. Additional work is still needed to improve the constitutive modeling of quasi-brittle rock failure under dynamic loading conditions, yet the methodology which was developed proved to be robust when studying the occurrence of unstable failures in highly stressed support rock.

3.0 Problem statement and objective

Unstable failures are observed in both coal and hard rock mines in deep mining conditions. Large unstable failures come in the form of massive collapses or cascading pillar failures. Slips along large discontinuity planes may also take place unstably which can cause significant damage to mine workings. More localized forms of unstable failures may affect smaller areas of a mine or even isolated sections of a single pillar or sidewall. Regardless of these different expressions of unstable failure, the phenomenon is classified at its fundamental level by a sudden release of stored potential energy which rapidly fails support rock and leads to a subsequent ejection of broken rock and debris into working areas of the mine. These unstable failures pose a serious risk to miners due to the violent ejection of broken material or from the resulting entrapment which it causes. This project addresses such violent unstable failures in terms of assessing their potential for occurrence and their expected intensity in deep coal mines.

The objective of the project is to develop numerical modeling methodologies for assessing unstable failures, which may manifest as rock bursts or coal mine bump events, in a given mine setting. This objective has been pursued through backanalysis studies of unstable failure events using the appropriate numerical modeling methodologies which we developed as part of our previous research on improving the understanding of unstable failure mechanisms. The current research explores unstable compressive failures in a coal seam and slip along pre-existing discontinuities such as coal – rock interfaces. Historical cases of bump events that occurred in coal and trona mines are considered for the backanalysis studies using the finite difference code FLAC3D and the distinct element UDEC code.

4.0 Research approach

The core of our research approach has been carrying out backanalysis studies of coal bump events using appropriate numerical models. This approach required furthering our previous modeling methodologies to include the calculation of energy released from rock bursts. We tested our new approach on various size single pillar models which were loaded under displacement or pressure loading conditions. Following a series of calibration processes, we developed several mine scale backanalysis simulations in FLAC3D and UDEC for assessing the magnitude of the energy released during unstable rock failure in coal and trona mines. The methodologies we have developed can be extended to other mines for backanalysis and rock burst assessment studies.

Historical research addresses the role of excess energy on the initiation and propagation of rockbursts, notably the seismic energy calculation by Duvall and Stephenson (1965), Energy Release Rate (ERR) concept introduced by Cook (1967), expanded upon by Salamon (1974), and Excess Shear Stress (ESS) presented by Ryder (1988). These methods address the energy released during the formation of an excavation and the hazard-amplifying effects of neighboring geological structures. Significant value has been gained by applying these design approaches using numerical methods to study specific mining geometries and in-situ conditions, yet neither approach accounts for brittle failure of the rock mass.

Our modeling efforts show that unstable failure conditions can be simulated in a mechanistically sound manner for brittle rock under excessive compression (Kias, et al., 2011; Garvey, 2013; Garvey and Ozbay, 2013) and sudden slip on fault planes or coal-rock interfaces under excessive shear loads (Gu, 2013;

Poeck, et al., 2015). The inclusion of such brittle behavior in numerical methods acceptably approximates rock failure and provides a method for directly evaluating unstable failure conditions as they emerge within mine models.

Numerical modeling of brittle material responses is infrequently applied to rockburst or coal bump studies. In most cases, the analysis is usually based on the strength to stress ratio of pillars without making specific references to bumps or rockbursts. Currently, there are no commonly accepted methods of quantifying the bump potentials of given mine layouts. The complexities involved in modeling brittle rock and in the estimation of rockmass properties make it extremely difficult to perform reliable analyses for assessing bump potential. Our recent studies in this area have progressed to a level that, using controlled numerical modeling methodologies, improved assessments of rock burst events can be made within the bounds of available *in situ* rock property data. The approach adopted involves detecting and quantifying unstable failures as they emerge within the model and calculating the released kinetic energy to determine the radiated seismic energy of failure events.

This report presents the processes developed in numerical models for simulating the progressive loading of a brittle rockmass or feature while calculating the associated energy changes within the system in realistic mine settings. The study considers two significant rock burst events, one coal and one trona mines, for detailed back-analysis studies. The modeling approach involves reducing the dynamic effects in the models from the loading procedure to nominal levels such that the any kinetic energy recorded in the model could be attributed to accelerations induced by unstable failure conditions. A dynamic energy balance is also used to determine the total kinetic energy that is damped out to return the model to static equilibrium. Both of these approaches provide straightforward methods for isolating the kinetic energy which is released from geomechanical systems as a consequence of unstable failure. Appendix I describes these energy calculations in more detail.

4.1 Crandall Canyon Mine Collapse

The Crandall Canyon coal mine collapse of 2007 is one of the most studied seismic events in coal mining history. A significant part of this report uses the information from the accident report published by Mine Safety and Health Administration, MSHA (Gates et al., 2008).

For the Crandall Canyon mine case, the three seismic events that occurred in 2007 are considered for the numerical modeling analyses. The first event occurred on March 10 in the North Barrier section during pillar retreat operation under 609 m of overburden (Figure 4.1). Over a dozen pillars sized 19 m wide x 22.5 m long were reported significantly damaged and a large volume of coal was ejected from the ribs to fill over half of the entry height with broken material (Gates et al., 2008). The seismic records from that day indicated that the failure produced a local magnitude event (M_L) of 1.8 (Pechmann, 2008).

The second event was a significantly larger collapse that occurred on August 6, 2007. Following the mining of the South Barrier section, a failure of roughly 0.2 km^2 of coal pillars occurred accompanied by a seismic event with a local magnitude of 3.9 (Gates et al., 2008). The extent of collapse was thought to be in close alignment with the collapse model developed by Pechmann et al. (2008) as shown by the dashed line in Figure 4.1.

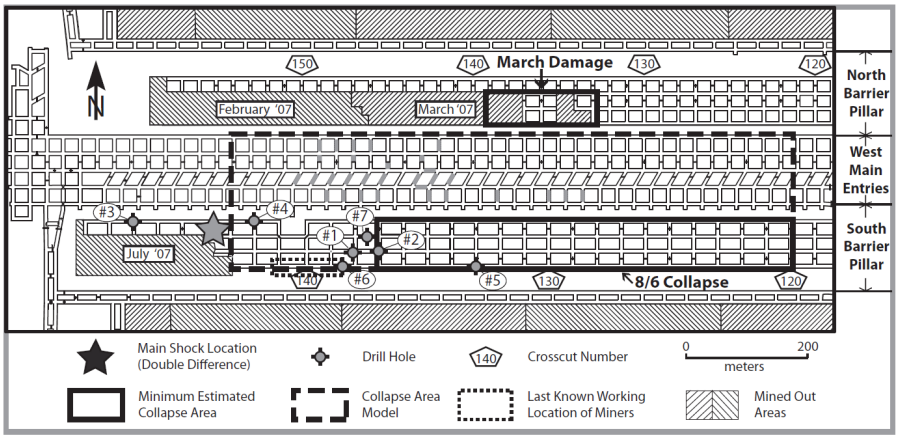

Figure 4.1 The panel at time of collapse with estimated collapse area shown by the dashed box (Pechmann et al., 2008)

Following the August 6 event, several coal bumps occurred during rescue operations led by MSHA. The rescue operations were halted following the fatal seismic event magnitude of 1.6 on August 16. An analysis of the seismic record, borehole observations, and subsidence data from the initial event (see Figure 4.2) confirmed that a section of coal pillars measuring approximately 0.2 km^2 in area failed in a rapid manner within a few seconds.

An extensive seismic analysis of the collapse indicated a compressive failure which fit well with a uniform crack closure model. Roughly 80% of the radiated seismic energy could be attributed to an implosion event (Ford et al., 2008), which may be simplified to a crack closing over an area of 920 m E-W by 220 m N-S with an average of 0.3 m vertical closure (Pechmann et al., 2008).

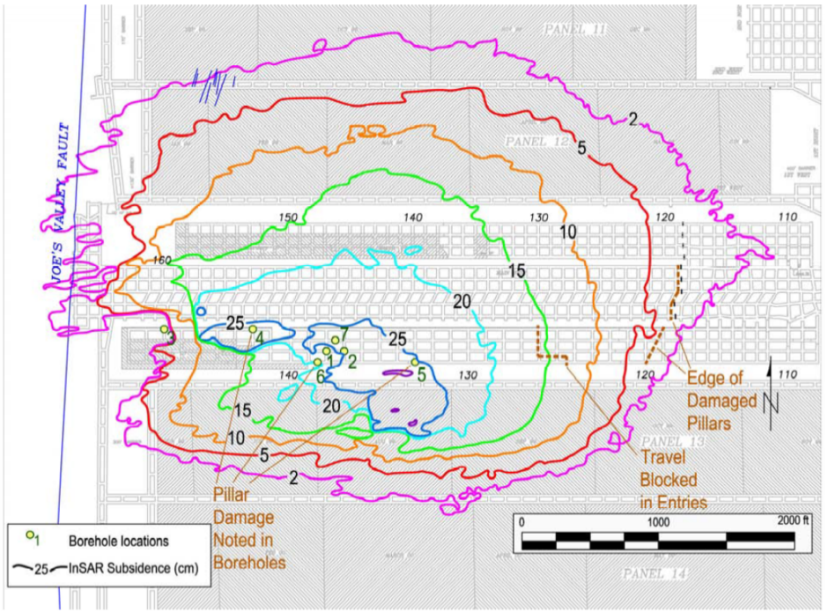

Figure 4.2 Surface subsidence contours in mm following the August 6 collapse

4.3 Model Calibration

The majority of the numerical simulations were carried out using the finite difference software FLAC3D (Itasca, 2013) and the distinct element software UDEC (Itasca, 2013). Coal material properties were calibrated to fit generalized strength parameters for coal with a compressive strength of 6.2 MPa. The elastic coal material properties shown in Table 4.1 were taken from the tests performed by Rao (1974) and Mishra and Nie (2013) on the Hiawatha coal seam. Elastic rock material properties were assumed for the rockmass above and below the coal seam and were derived from values given by Pariseau (2011).

Table 4.1 – Elastic material properties assigned to coal and surrounding rockmass

Material Property	Value
Young's Modulus (coal)	3 GPa
Poisson ratio (coal)	0.2
Young's Modulus (rockmass)	23.4 GPa
Poisson ratio (rockmass)	0.3

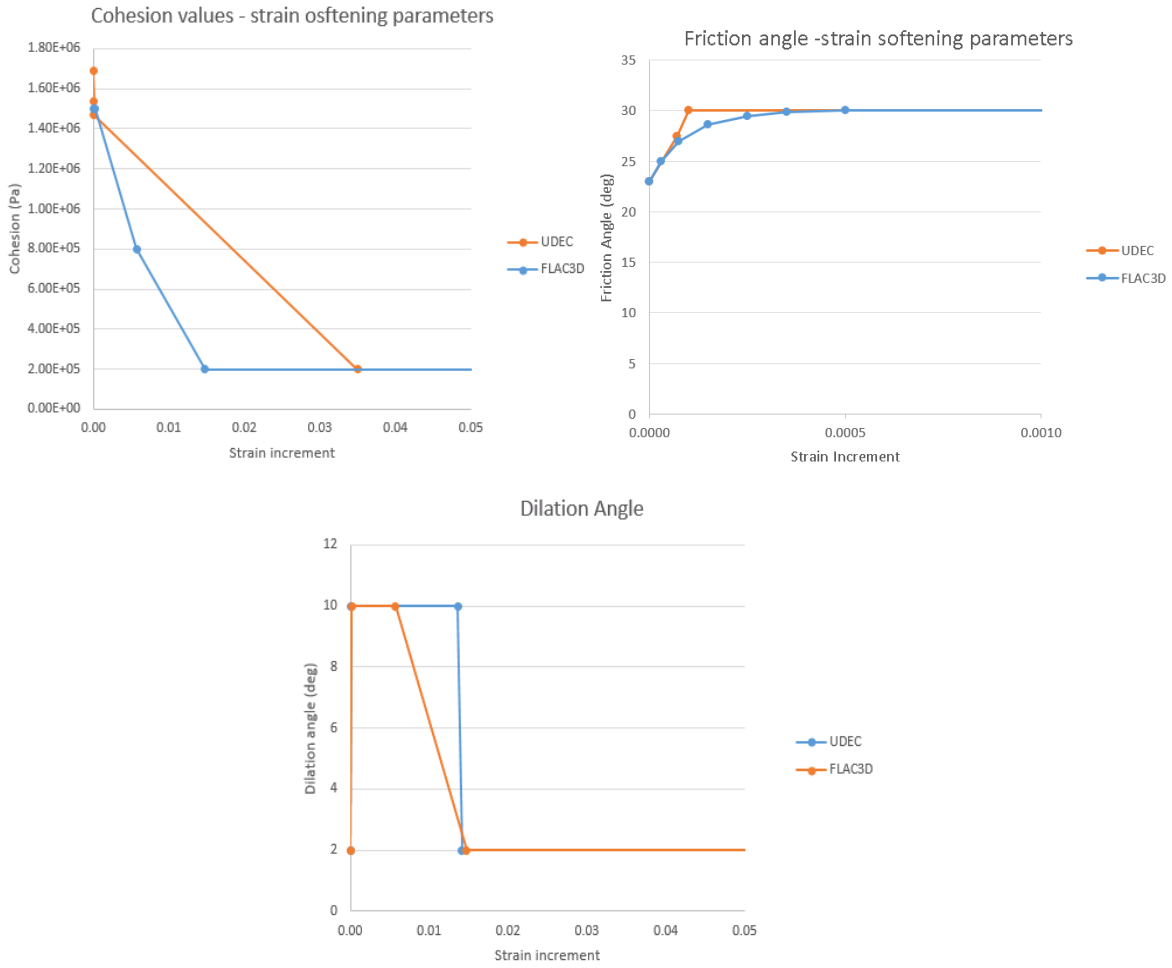

Figure 4.3 Mohr-Coulomb Strain-Softening inputs for FLAC3D and UDEC

The uniaxial compressive strength of coal seam for the models was developed from a width-to-height ratio 0.5 specimen. The post-peak modulus was calibrated to be around -3 GPa although this portion of the stress-strain response remained non-linear in the case of FLAC3D.

A Mohr-Coulomb strain-softening constitutive model was used to achieve brittle stress-strain characteristics of coal. The calibrated inputs for the strain-softening model are provided in Figure 4.3 and fit a standard cohesion-weakening, friction-hardening response of a dilatant material.

Calibration procedures were performed separately in FLAC3D and UDEC due to the subtle differences introduced by meshing schemes employed by each of the software packages. Two sets of similar input parameters were derived for cohesion, friction angle, and dilation angle as functions of plastic strain.

4.4 FLAC3D simulations

Isolated coal pillar models were constructed in FLAC3D in both two- and three-dimensional configurations. Figure 4.4 shows these coal pillars in red between the sandstone rock mass in blue. First a range of pillar width-to-height ratios were tested to compare strength values against empirical formulae. An applied pressure boundary was then used to simulate the widespread collapse of an infinite array of similarly-sized pillars. The ratio of excess energy to energy applied through the loading process relates to the ratio of radiated seismic energy to change in potential energy in a collapse case.

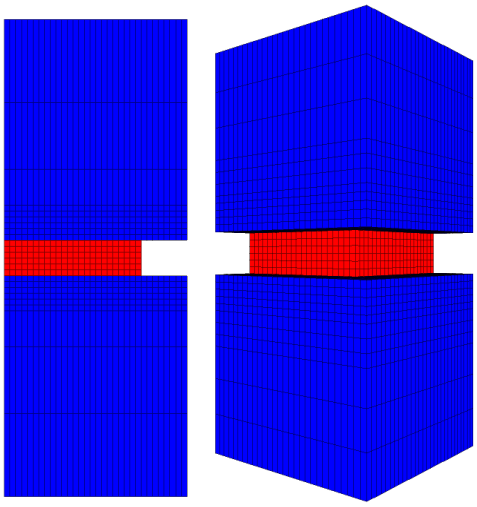

Figure 4.4 Two- and three-dimensional pillar models in FLAC3D

The pillars were loaded by applying vertical compression at the top and bottom of the sandstone blocks while restricting the horizontal expansion on all sides except at the pillar face. The shear strength of the coal–sandstone contact surfaces were made to be infinitely strong. The tests were repeated for coal pillars with width-to-height ratios ranging from 1 to 8. Figure 4.5 shows the stress-strain behavior of the pillar models and Figure 4.6 shows that the model pillar strength compares well against the Mark-Bieniawski and Salamon-Munro pillar strength formulae (Mark, 1990, Salamon and Munro, 1967). The coal material properties of these pillars were used for all the FLAC3D models in the remainder of this report.

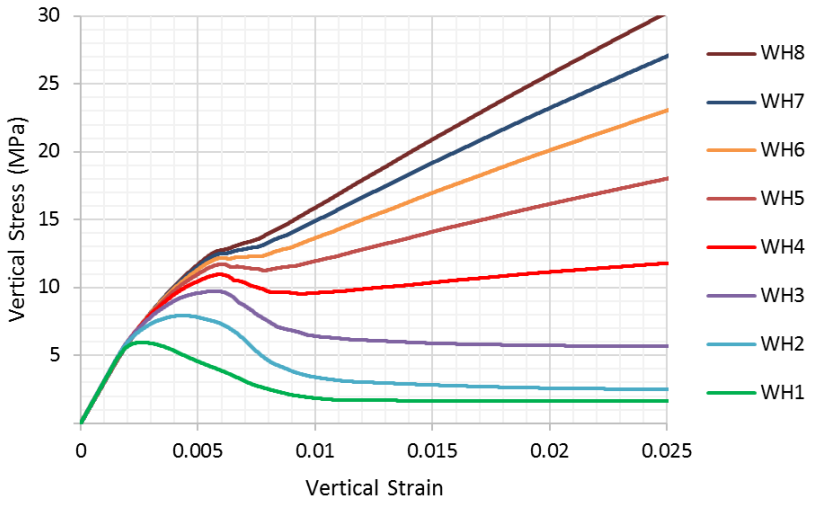

Figure 4.5 FLAC3D stress vs. strain behavior of two-dimensional pillar models with varying w:h ratio

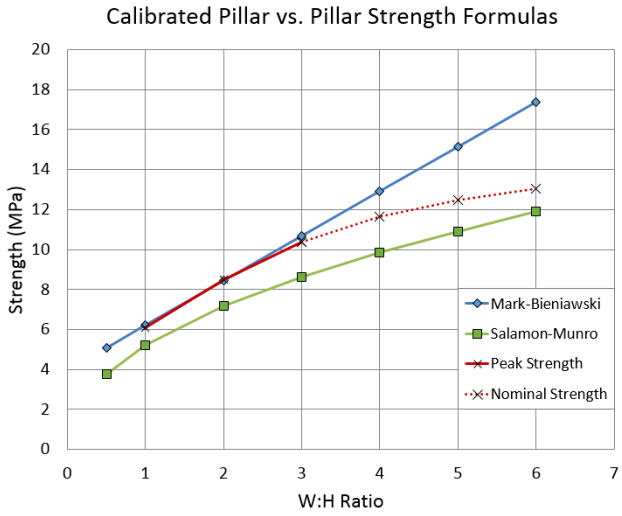

Figure 4.6 3D Pillar Strength Results as Compared to Mark-Bieniawski and Salamon-Munro Pillar Strength Formulas (assumes height = 2.4 m). Nominal strength in the graph refers to the first peak in the high width-height ratio pillars.

4.5. FLAC3D single pillar tests

Tests were conducted in FLAC3D to establish the performance of the individual Crandall Canyon pillar geometries under varied loading conditions. To simulate a rigid loading system, a displacement-based loading scheme was adopted where compressive stresses were very slowly added to the pillar through applications of displacements along the upper surface of the system. This displacement-based approach is given the term "local" loading because it represents the loading system stiffness applied onto a single pillar due to elastic rebound of the immediate roof and floor. A second loading scheme was adopted to

apply a pressure boundary onto the upper surface of the system. The pressure was increased in a quasi-static manner as compression was applied onto the pillar. This pressure was approximately constant during periods of unstable failure and thereby represented a perfectly soft, horizontal load line. The pressure-based loading application was given the term "global loading" since it represented the loading system stiffness of an infinite array of similarly sized pillars failing under a constant deadweight from the overburden. A range was thereby established for the failure response of the pillar models under both very stiff and perfectly soft loading system stiffnesses.

Three different pillar geometries with infinitely strong coal-rock interfaces shown in Figure 4.7 were tested under these conditions to represent 1) the 2.4m tall pillars in the North barrier section, 2) the 2.4m tall pillars in the South barrier section, and 3) the 4m tall pillars in the South barrier section after 1.4m of floor coal was mined during the retreat of the neighboring pillars. The results from the FLAC3D simulations of local loading tests yielded the characteristic stress-strain behavior of the three pillar types shown in Figures 4.8 and 4.9. The 2.4 m tall pillars appear punching into floor coal while 4 m tall pillar exhibits a gradual failure.

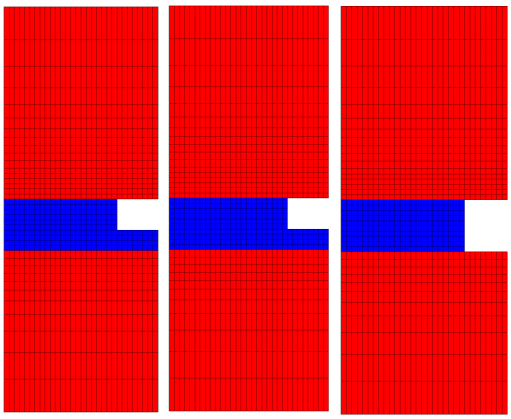

Figure 4.7 FLAC3D Crandall Canyon models to test pillar geometries from North Barrier section, South Barrier section, and South Barrier section during retreat

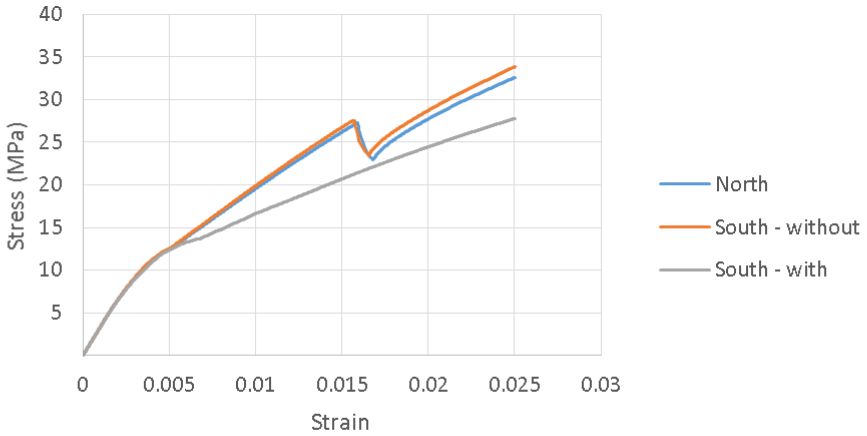

Figure 4.8 FLAC3D two-dimensional pillar stress vs. strain for pillar geometries in North Barrier, South Barrier, and South Barrier with bottom coaling during retreat

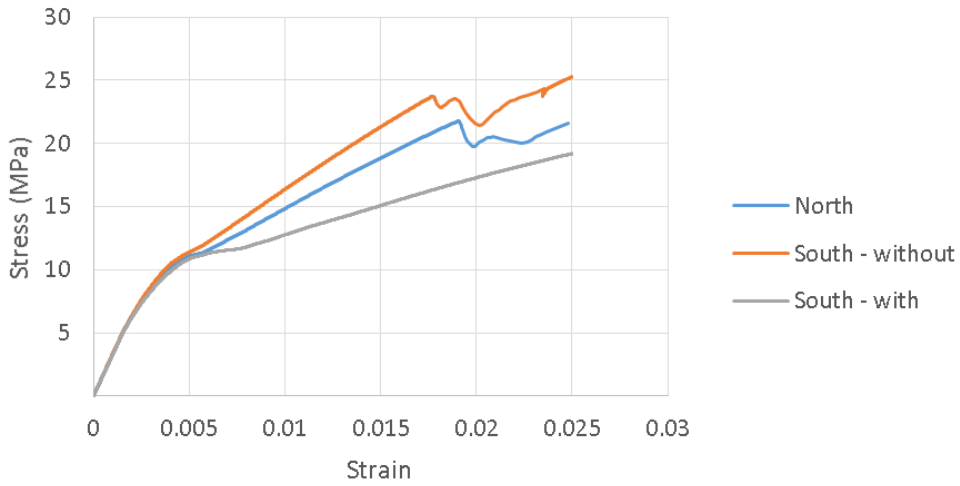

Figure 4.9 FLAC3D three-dimensional pillar stress vs. strain for pillar geometries in North Barrier, South Barrier, and South Barrier with bottom coaling during retreat

4.5.1 FLAC3D single pillar energy results

Our proposed energy balance, which is outlined in Appendix I, was applied to these models to calculate the excess energy released during unstable failure conditions. Elastic, Mohr-Coulomb elastic-perfectly plastic, and Mohr-Coulomb strain-softening constitutive models were tested in FLAC3D. The unstable excess energy results from the two- and three-dimensional simulations, including those in Figures 4.8 and 4.9, are given in Figures 4.10 and 4.11 in terms of total energy released in Joules per square meter of roof area supported by the pillar. This unit of J/m^2 provides a normalized value of excess energy to more directly compare two- and three-dimensional pillar results.

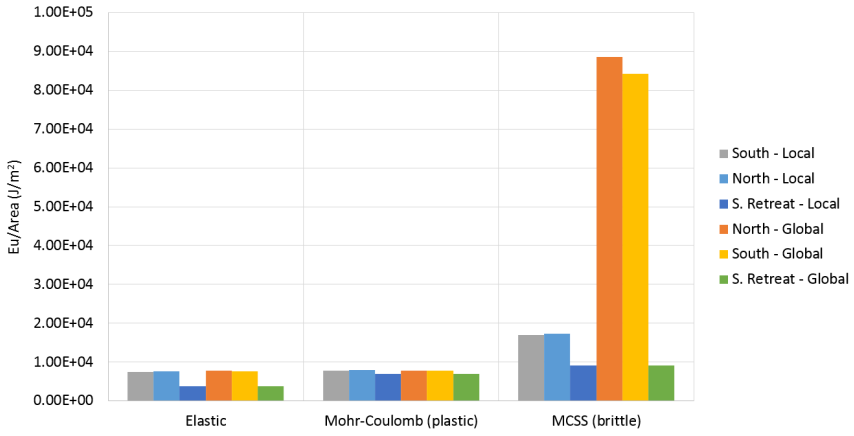

Figure 4.10 2D Pillars in FLAC3D showing excess energy values normalized over the planar area of support

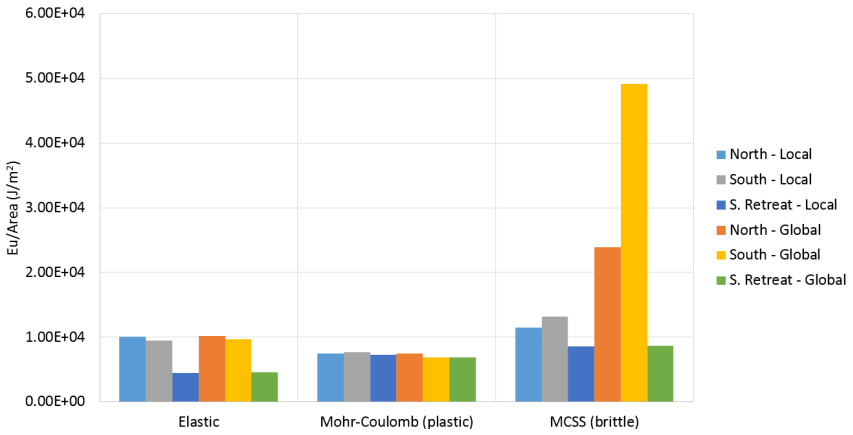

Figure 4.11 3D Pillars in FLAC3D showing excess energy values normalized over the planar area of support

For elastic and Mohr-Coulomb plasticity models, all Crandall Canyon pillar geometries resulted in small magnitudes of unstable excess energy (see Appendix I for description energy terms) generated from the quasi-static, yet non-zero, FLAC3D grid point velocities which are introduced due to the applied loading procedure. These magnitudes indicated no unstable failure and minimal kinetic energy released from the system. However, the results of the Mohr-Coulomb strain-softening pillars revealed much about the localized failure of a single pillar and widespread collapse of similarly sized pillars. The normalized excess energy magnitudes were seen to be higher in the two-dimensional case due to the more significant drop in stress during failure for these models. The stiff, local loading system resulted in slightly elevated magnitudes of excess energy for the brittle models as compared to the elastic and perfectly plastic Mohr-Coulomb cases. The global loading condition released more excess energy during pillar failure as is expected from the softer loading system. These results of the global loading condition correspond to the highest excess energy which may be released from the system unless dynamic impact loading is also considered within the models.

A useful value for studying the pillar models comes from the ratio of unstable excess energy to total external boundary work (Eu/Wb). This value corresponds to the ratio of radiated seismic energy to the total energy released through changes of potential energy or stored strain energy. This energy ratio is commonly referenced as seismic efficiency in traditional fault slip analysis and has also been estimated in several cases of mining induced seismicity (McGarr, 1994). The values of Eu/Wb were calculated over the duration of the FLAC3D single pillar tests and are reported in Figures 4.12 and 4.13 for all material models.

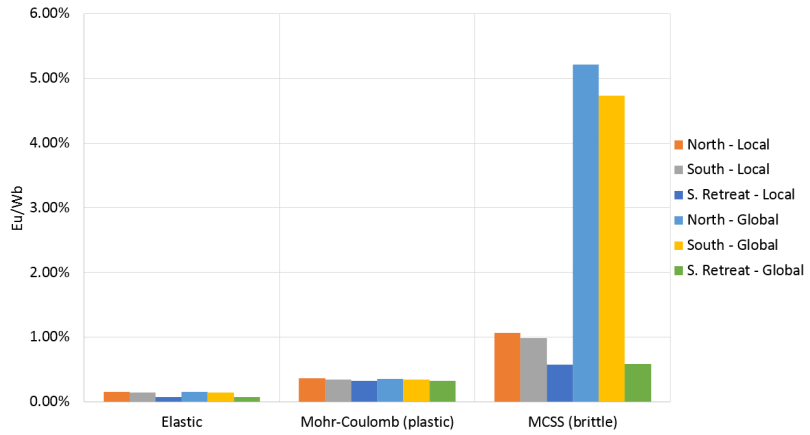

Figure 4.12 FLAC3D 2D Pillars showing ratio of unstable excess energy to total boundary work

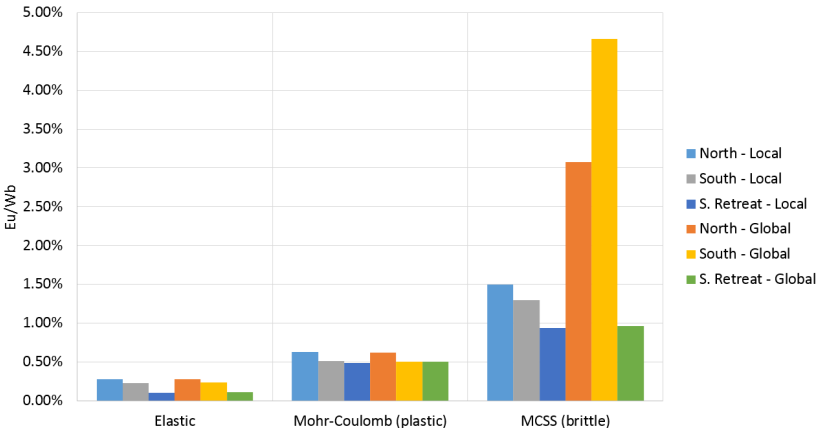

Figure 4.13 FLAC3D 3D Pillars showing ratio of unstable excess energy to total boundary work

The percentage of unstable excess energy to total boundary work ranged from 0.58% to 5.21% for the 2D quasi-brittle pillar models in FLAC3D. The case of a more slender south barrier pillar resulted in the lowest magnitudes of energy released under both local and global loading conditions (0.58%) whereas the north barrier geometry yielded the highest magnitudes (5.21%) under full overburden loading conditions.

4.5.2 Energy validations in FLAC3D pillar model simulations

No unstable failure was observed in the 4m high pillar to represent the south barrier pillars after the bottom coal from neighboring pillars had been removed. One important aspect which is not accounted for within this analysis is the transition of a pillar geometry from the squat south barrier pillars to the more slender geometry found during the retreat operation. This transition from a squatter to a slenderer geometry can potentially cause unstable failures. The effect of this active removal of confinement requires additional analysis.

The 3D pillar results mirrored those of the 2D analysis in that unstable failure was observed in the case of the squat pillars following north and south barrier pillar development. The largest magnitudes of unstable excess energy (Eu/Wb = 4.66%) were seen to be released in the case of the south barrier pillar if widespread collapse was simulated in the pillars formed in development. Once again, no instability

was observed in the case of the more slender south barrier pillars after the removal of neighboring floor coal, however this analysis does not account for the transition from a squat to a more slender geometry.

A second formulation of Eu/Wb was then used to find the ratio of excess energy to work done by the loading system as calculated exclusively during periods of instability. The magnitude of excess energy to boundary loading work is invariably higher during periods of instability and these values established an upper limit for these ratios. The unstable excess energy is shown as a percentage of the total boundary work in Table 4.1 with values given both over the entire test and exclusively for the periods of instability.

Table 5.2 FLAC3D results for ratio of excess energy to total boundary loading work

	Average	During instability
2D Eu/Wb (North)	5.21%	21.4%
2D Eu/Wb (South w/)	0.58%	*
2D Eu/Wb (South w/o)	4.73%	8.9%
3D Eu/Wb (North)	3.08%	8.7%
3D Eu/Wb (South w/)	0.96%	*
3D Eu/Wb (South w/o)	4.66%	14.2%

*No unstable failure was observed in these tests

When the numerical results were analyzed to include only the period of unstable failure of the pillars within the South Barrier Pillar, the percentages of unstable excess energy to total boundary work were found to increase to a maximum of 21.4% in the case of the two-dimensional pillar geometry from the North Barrier section. The energy ratios from pillars in the South Barrier section where coal had been removed from the floor were unchanged since no portions of instability could be identified.

4.6. Energy validations in UDEC Crandall Canyon simulations

The modeling procedure for simulating failure of single pillars was repeated using UDEC. In the UDEC models, the added variations of constitutive model were applied to the rock-coal interface above and below the seam. The results from the wide and narrow pillars are separately discussed below.

4.6.1 Single Pillar Tests

A total of 27 variations of material models were built to include the three different pillar geometries shown in Figure 4.14 and three different materials each for the continuum coal material and for the coal-rock interface. As in the FLAC3D models, two loading system stiffnesses were used to represent rigid loading via a displacement based application of loads and soft loading through a pressure based application of loads. These variations of geometry, coal material, interface material, and loading system stiffness brought the total number of UDEC single Crandall Canyon pillar tests to 54.

The resulting unstable excess energy was calculated from the sum of kinetic energy and damped work. This dynamic energy balance was taken in lieu of the quasi-static calculation of unstable excess energy due to added difficulties of calculating the static energy components in UDEC. The static and dynamic

energy balances yielded identical solutions for unstable excess energy. The combined results from these single pillar tests are shown as Figure 4.15.

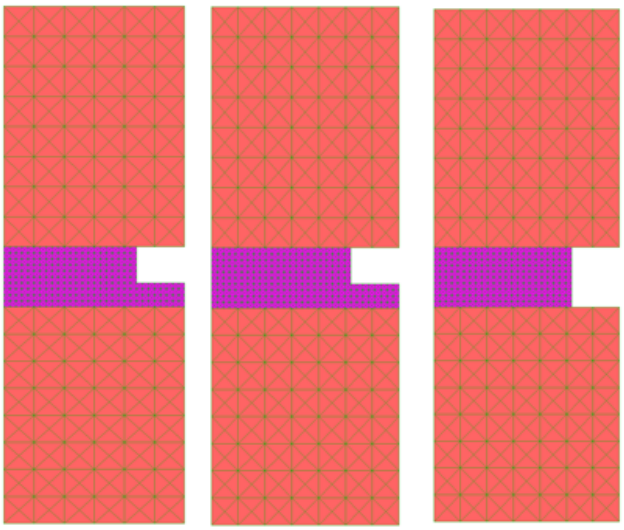

Figure 4.14 UDEC single pillar model showing north barrier, south barrier, and south barrier pillar geometry developed from bottom coaling during retreat mining

Like in the FLAC3D analysis, two stable material types were applied to represent the coal seam in order to determine the kinetic energy produced through the loading process alone. The stable material types were taken to be elastic and Mohr-Coulomb plastic behavior. Similarly, a Coulomb-slip model was applied to the interface to include the possibility of stable slip along an interface. Figure 4.15 shows the results of these material combinations where the first letters refer to the material type applied to the coal and the second refer to the interface material (note that MC refers to the Coulomb-slip type interface). The velocity loading condition was used to establish a lower limit for the energy released during failure due to the relatively high loading system stiffness. These results were contrasted through the pressure loading condition which provided an upper limit for the magnitude of energy which could be released during widespread collapse of similarly sized pillars.

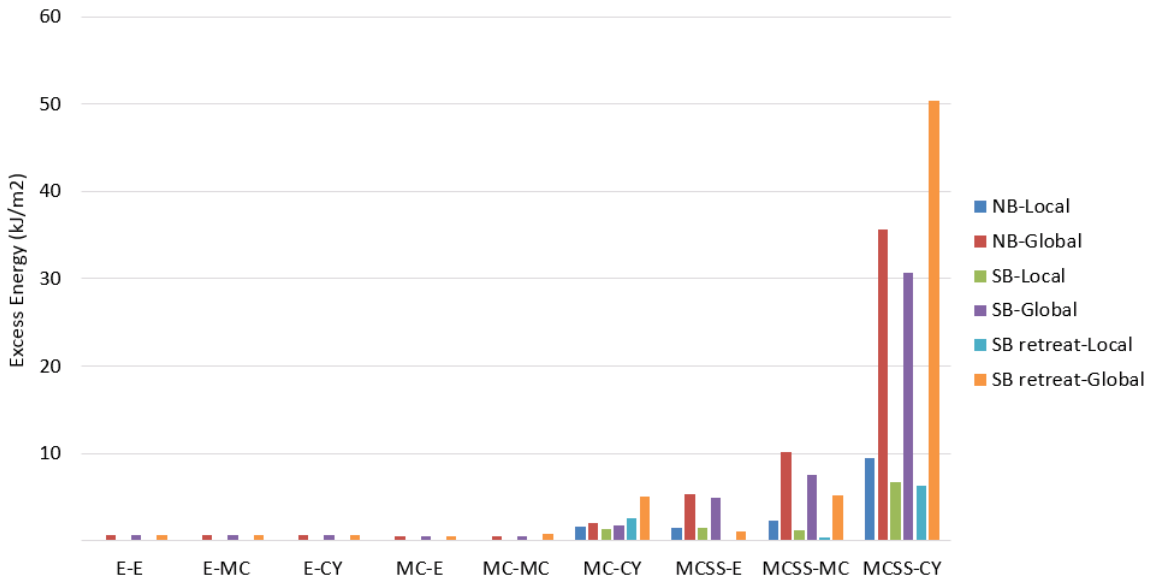

Figure 4.15 Kinetic energy released in UDEC single pillar tests where coal material is taken as E, MC, or MCSS and the coal-rock interface is given E, MC (Coulomb-slip), or CY joint characteristics (CY is Continuously Yielding joint model for contact shear failure in UDEC (Itasca Consulting Group Inc. (2013))

These results show that kinetic energy magnitudes remained small for all perfectly stable material combinations. The energy also remained low in the Elastic E and Continuously Yielding CY (E-CY in Figure 4.15) case, or where an elastic coal was bedded between continuously-yielding joints, which indicated that no sudden slip occurred in the joint model. However, when a Mohr-Coulomb model was used in combination with a CY model, the kinetic energy was seen to increase significantly. Further, as the brittleness of material combinations increased, so too did the release of energy. The MCSS coal with CY joint behavior was seen to release by far the largest magnitudes of kinetic energy during failure which corresponded with the highest levels of instability experienced within the tests.

The North and South Barrier pillar geometries showed comparable energy magnitudes for all tests, with the slightly wider South Barrier geometry yielding lower magnitudes of released kinetic energy. The more slender South Barrier pillar geometry developed due to bottom coaling while retreating neighboring pillars showed lower energy magnitudes than its counterparts under the velocity loading condition. However, the pressure loading condition was seen to release more kinetic energy when a continuously-yielding joint model was used. This indicates that unstable failure was less likely to occur in the more slender pillar geometry. Also, upon failure initiation, the South Barrier pillar with bottom coaling consumed less energy during failure when sudden slip was incorporated along the interface.

These results were further outlined in the context of the ratio of kinetic energy released to the total energy added to the system during failure. These values are listed in Table 4.3 where the MCSS coal with fixed interface may be compared against the FLAC3D energy results. The MCSS coal with CY interface then indicates these energy ratios for the model with the highest recorded levels of unstable failure.

Table 4.3: Ratio of kinetic energy to total energy added to system in single pillar tests

Cases			Eu/Wb (Average)	Eu/Wb (During Instability)
1	NB Pressure	MCSS-E	0.85%	4.38%
		MCSS-CY	4.35%	6.45%
2	SB Pressure	MCSS-E	0.50%	3.55%
		MCSS-CY	3.21%	4.86%
3	SB Bottom Pressure	MCSS-E	0.02%	0.40%
		MCSS-CY	6.67%	9.41%

The pressure boundary represents an idealized loading case where a constant pressure is being applied over an infinite array of pillars. The energy ratios from these UDEC tests indicate that the MCSS-CY model released much more of its total energy in the form of unstable excess energy as compared to MCSS-E tests. The results listed in Table 4.3 are taken from compression tests run to 0.025 pillar strain as in the case of the FLAC3D single pillar tests. These UDEC energy results do not include potentially high levels of instability which were experienced after additional compression. For the three MCSS-CY models which are referenced, unstable failure was seen to continue at the conclusion of the tests and the models were not in a state of static equilibrium when energy results were tabulated. The MCSS-E models were also seen to experience large magnitude instabilities after the 0.025 strain value had been reached. The results from these analyses should be supplemented through additional studies of unstable failures in squat coal pillars in order to develop more appropriate techniques for assessing instability.

4.7 UDEC modeling of large width/height pillar tests

According to the conventional understanding of pillar responses, as presented in Figures 4.5 and 4.6, pillars with width-to-height ratios of 5 or more are unlikely to reduce in strength during inelastic deformation due to their highly confined and hardening cores (Das, 1986). These squat pillars yet do experience bumps and have been shown to reduce significantly in strength under unstable loading conditions (Iannacchione, 1990). The Crandall Canyon case can attest to this fact and even demonstrated large portions of a strip pillar with a width-to-height ratio of 15 failing dynamically.

The continuum-based representation of pillars in FLAC3D models prove capable of capturing localized failures at the pillar *ribs* yet the coal support structures maintained their overall strength with known *in situ* coal properties applied to the seam. A more realistic representation of pillar behavior in the Crandall Canyon case would include a finite strength for the coal-rock contact. More extensive pillar failure also becomes possible by introducing shear slip along this surface. If a more realistic failure mode is incorporated for the contact, such as through a displacement-weakening constitutive model, then a reduction of shear stress occurs with the initiation of sliding across this surface. In the highly confined conditions found within squat pillars, a sudden reduction in shear stress across coal-roof contacts leads to a significantly more violent and widespread failure within the pillar. All of these

behaviors stem from known material characteristics; however the combination of these quasi-brittle failure modes within a single model appear to have been less studied than the cases with perfectly plastic contact conditions.

4.7.1 Pillar-roof contact properties

We conducted a series of tests in UDEC to analyze shear slip along the rock-coal contact as a potential mechanism for triggering large coal bump events within pillars of squat geometries. Two forms of slip were explored: 1) the stable slip along an interface with constant peak strength and 2) the sudden, unstable slip of a discontinuity with a drop of shear stress during failure. The strength properties of the interface which are listed in Table 4.4 were calibrated in UDEC using a Coulomb slip model to represent stable slip and the inputs in Table 4.5 for a continuously-yielding joint model to simulate unstable slip. The resulting behavior of the interface is shown in Figure 4.16 in terms of the shear stress vs. shear displacement records obtained during a controlled direct shear test.

Table 4.4 Coulomb-slip joint model parameters

Description	Value	
Joint normal stiffness	50	GPa/m
Joint shear stiffness	50	GPa/m
Joint cohesion	0	GPa
Joint friction angle	20	deg.
Joint dilation angle	0	deg.
Joint tensile strength	0	GPa

Table 4.5 Continuously-Yielding joint model parameters

Description	Value	
Joint normal stiffness	50	GPa/m
Joint shear stiffness	50	GPa/m
Joint normal stiffness exponent	0	-
Joint shear stiffness exponent	0	-
Joint intrinsic friction angle	15	deg.
Joint initial friction angle	40	deg.
Joint roughness parameter	0.15	mm

The inclusion of an interface capable of failure did little to change the ultimate strengths of the pillars, however the pillars' post-failure behavior was drastically altered due to the slip at the coal-rock contact. The pillar post-failure weakening effect was much greater in the case of the Continuously-Yielding joint model as a result of the reduction in pillar stress bearing capacity as compared to the case of the Coulomb slip model. Large portions of the coal pillar were seen to rapidly lose their strength with the sudden drop of confining pressures. Individual pillar behavior and the overall response of the mining layout were both affected due to this reduction in post-peak strength once slip was initiated.

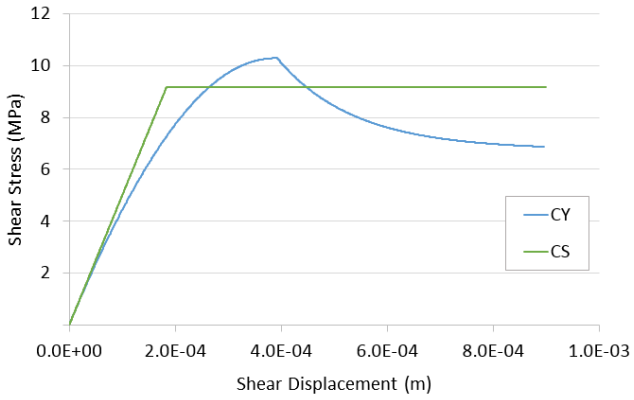

Figure 4.16 Shear stress vs. shear displacement of Continuously-Yielding (CY) and Coulomb slip (CS) constitutive models applied to the rock-coal interface

4.7.2 UDEC pillar tests

Each joint constitutive model was tested to confirm that the peak strengths of the pillar models approximated the pillar strength determined using the Mark-Bieniawski formula. The results from these tests are shown in Figure 4.17 for the Continuously-Yielding joint model used in conjunction with a Mohr-Coulomb strain-softening model to represent coal. The peak pillar strengths are reported against the Mark-Bieniawski pillar strength formula in Figure 4.18 where an infinite pillar length and 6.2 MPa compressive strength was assumed for the empirical formula.

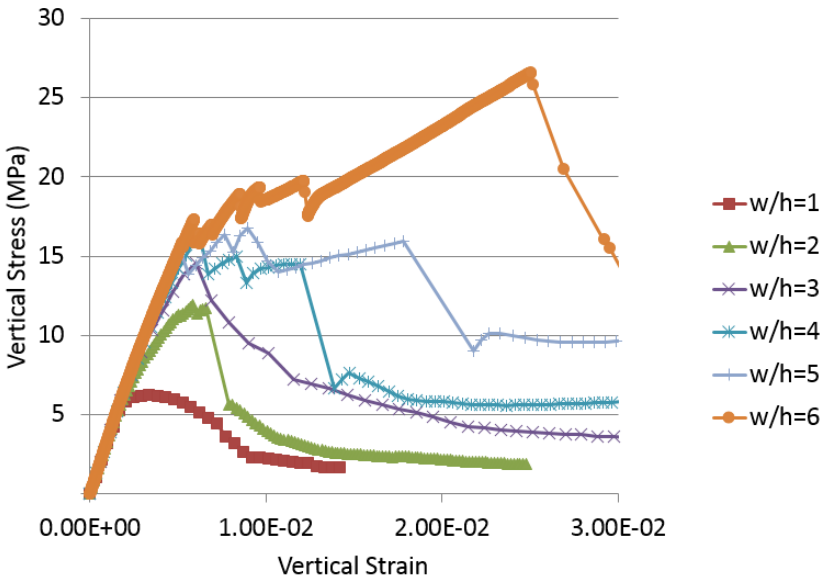

Figure 4.17 Two-dimensional vertical stress-strain behavior of UDEC pillars with CY joints at contacts

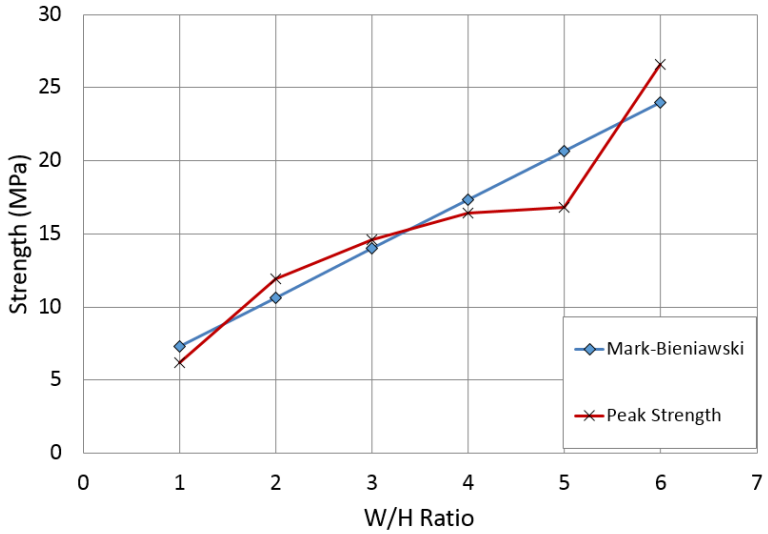

Figure 4.18 Comparison of MCSS-CY pillar strength and Mark-Bieniawski pillar strength formula

The MCSS-CY pillar strengths shown in Figure 4.18 are in relatively good agreement with the Mark-Bieniawski pillar strength formula where an infinite length is assumed for the in-plane direction. There is one unexpected result in the case of the pillar with a width-to-height of 5. The strength of this pillar is less than expected from the increasing trend of pillar strengths. We believe that this discrepancy is an example of the non-unique nature of brittle failures. For any strain-weakening material, the stresses and displacements may take different paths during loading due to small changes in initial conditions. To address this issue, any study which focuses on realistically simulating strain-weakening effects should take a parametric or stochastic approach to determine a range of likely behaviors, rather than assuming the correctness of a single solution.

4.8 Mine models

The mine scale analysis was conducted on a two-dimensional cross-section of the collapsed portion of the Crandall Canyon mine. Simulations are repeated for both FLAC3D and UDEC. Mining steps were simulated starting from an intact seam of coal and progressing to a state after the massive collapse on August 6. These models were studied to determine periods of instability and to correlate the released excess energy to magnitudes of radiated seismic energy in the coal bump cases outlined in the Background section of this report.

The model geometries used for the simulations are shown in Figure 4.19. Plane strain models were constructed in FLAC3D with an in-plane depth of 0.4 m such that cubic zones could be used for the meshing of the coal seam. The UDEC model also had a plane-strain assumption but its in-plane depth was a unit value of 1 m.

Abutment loads were simulated through the application of forces along the left and right sides of the models (Figure 4.20). Total abutment loading was equal to a 21° abutment angle in agreement with the ALPS database (Mark, 1990) for the given overburden density of 2,350 kg/m^3 and an average depth of overburden of 609 m.

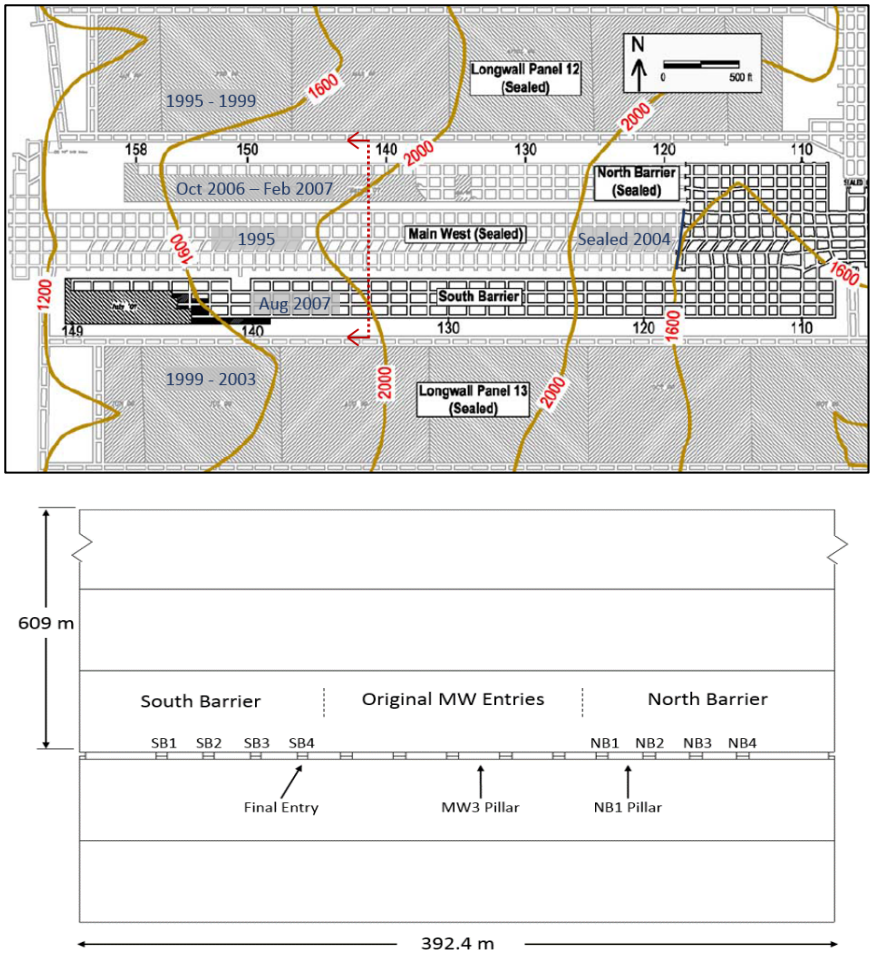

Figure 4.19 Model geometry used for the simulations. Dashed red line in the plan view above shows the location of modeled cross-section in the sketch below.

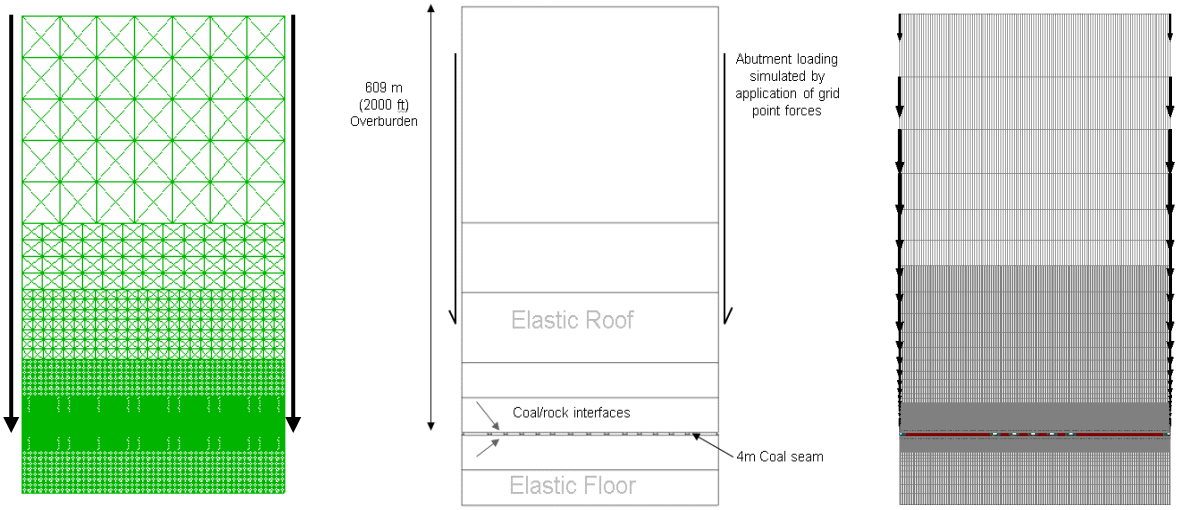

Figure 4.20: Abutment geometry used for the simulations: UDEC, simplified sketch, and FLAC3D.

An elastic model was first constructed of an abutment wedge with a horizontal restraint along its length. The shear forces applied by the wedge were re-applied onto the full mine model as gridpoint forces. The vertical loads representing the abutment are presented in Figure 4.20.

This approach of modeling the abutment load distribution was assessed by comparing the load transfer distance at the seam level with distances calculated in a recent study (Larson and Whyatt, 2012) of an instrumented longwall panel in a deep western U.S. coal mine whose lithology was similar to that of Crandall Canyon. A 90% load transfer distance of 200m was found for the models which compared well with results from the instrumented panel.

Empirical relationships establish that the approximate distance for total load transfer is approximately 1.86 times that of the 90% load transfer distance (Peng and Chiang, 1984). From this relation the distribution of abutment stresses onto the coal seam could be compared against the empirical formula shown in the equation below (Mark, 1990) where D is the full extent of abutment stress generated by the load L_s.

$$\sigma_a(x) = \frac{3L_s}{D^3}(D - x)^2$$

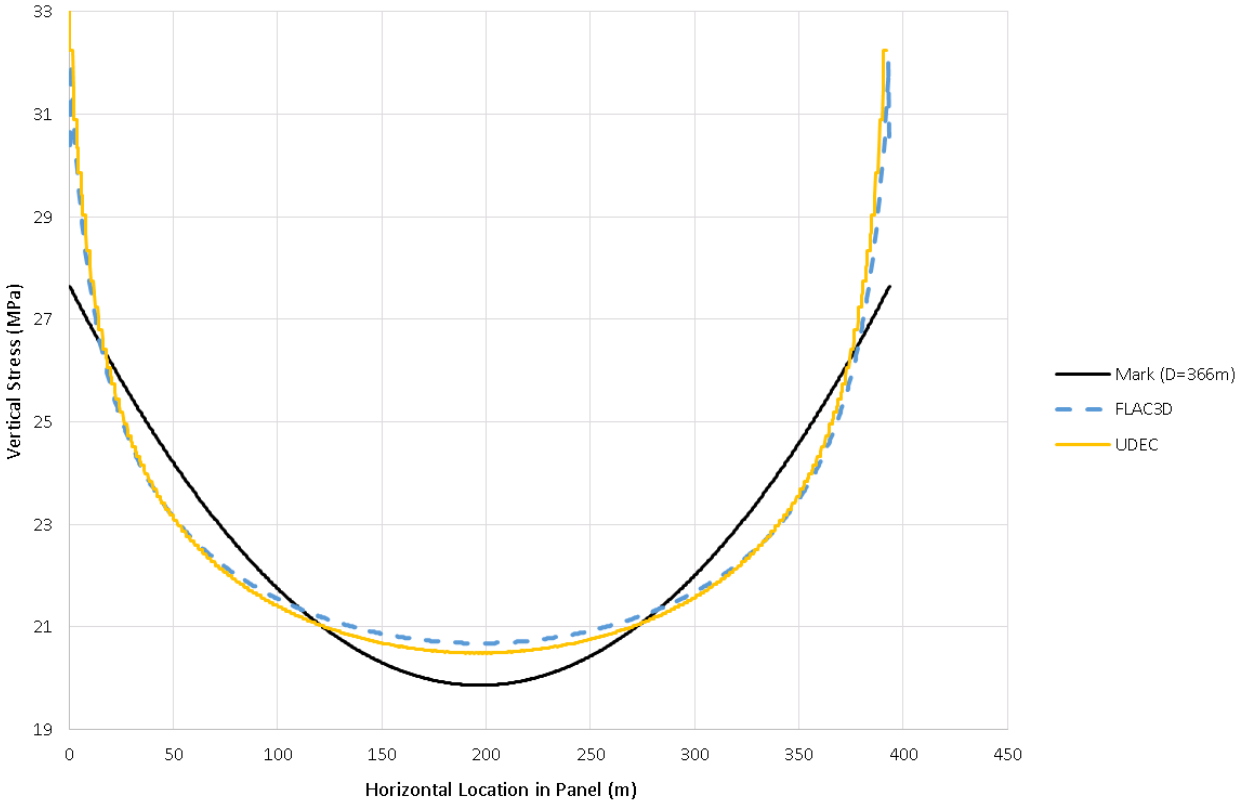

Figure 4.21 Vertical stresses generated by abutment model compared against the one by Mark (1992) for calculating abutment load distribution in the seam

The distribution of vertical stresses in FLAC3D and UDEC are plotted out in Figure 4.21 against the results of the empirical formula where the total load transfer of 366 m corresponds with a 90% load transfer distance of 200m. The high stress concentrations on the sides of the numerical models are a result of the elastic assumptions made for the coal seam. The applied abutment forces which were calculated from the elastic wedge model were taken for the remainder of the mine-scale analysis as an approximation of the neighboring longwall panels.

The overburden and floor strata were assumed to be elastic based on a number of observations made by miners before and during the massive collapse. Seismic source analysis indicated that the roof and floor converged uniformly in the August 6 massive failure (Ford et al., 2008). Massive sandstone units in the roof were capable of transmitting loads across large distances of the mine and there were multiple examples of the relative strength and stiffness of the roof strata above the Crandall Canyon mine. Large cantilevers had been seen to extend into retreated areas and poor breakage of the roof was common (Gates et al., 2008). Complete recovery of the adjacent longwall panels eliminated the potential for strata from the North and South to resist downward motion above the Main West panel. The collapse mode was therefore taken as purely vertical closure in the numerical models while assuming no failure in the overburden strata.

The pillar geometries and extraction sequences were identical between the FLAC3D and UDEC simulations. In its final state, the FLAC3D model geometry approximated the cross-section shown in Figure 4.22. The overburden depth was taken as the average depth of 609 m over the collapsed area proposed by (Pechmann, et al. 2008). A slow removal of coal material was initiated within an unmined seam with an initial extraction height of 2.4 m. Slender 0.4 m slabs were removed sequentially from the excavation area while applying forces along the internal boundary to control the unloading process.

The development stages took the order in following order:

1. Excavation of Main West entries 1 – 5
2. Application of abutment load on south boundary of model
3. Application of abutment load on north boundary of model
4. Excavation of entries 1 – 4 in north barrier
5. Retreat mining of two pillars in north barrier
6. Excavation of entries 1 – 4 in south barrier

Closures were controlled by applying forces onto the excavation surface which were equal to the pre-mining tractions. These forces were then reduced over 100 steps while allowing the model to come to equilibrium between reductions in force.

An extended study was conducted on the role of interface slip in the expression of unstable failures by modeling interfaces both above and below the coal seam in UDEC. These two interfaces were assigned

elastic, Coulomb-slip, and Continuously-yielding joint constitutive laws whose input parameters were identical to the single pillar tests.

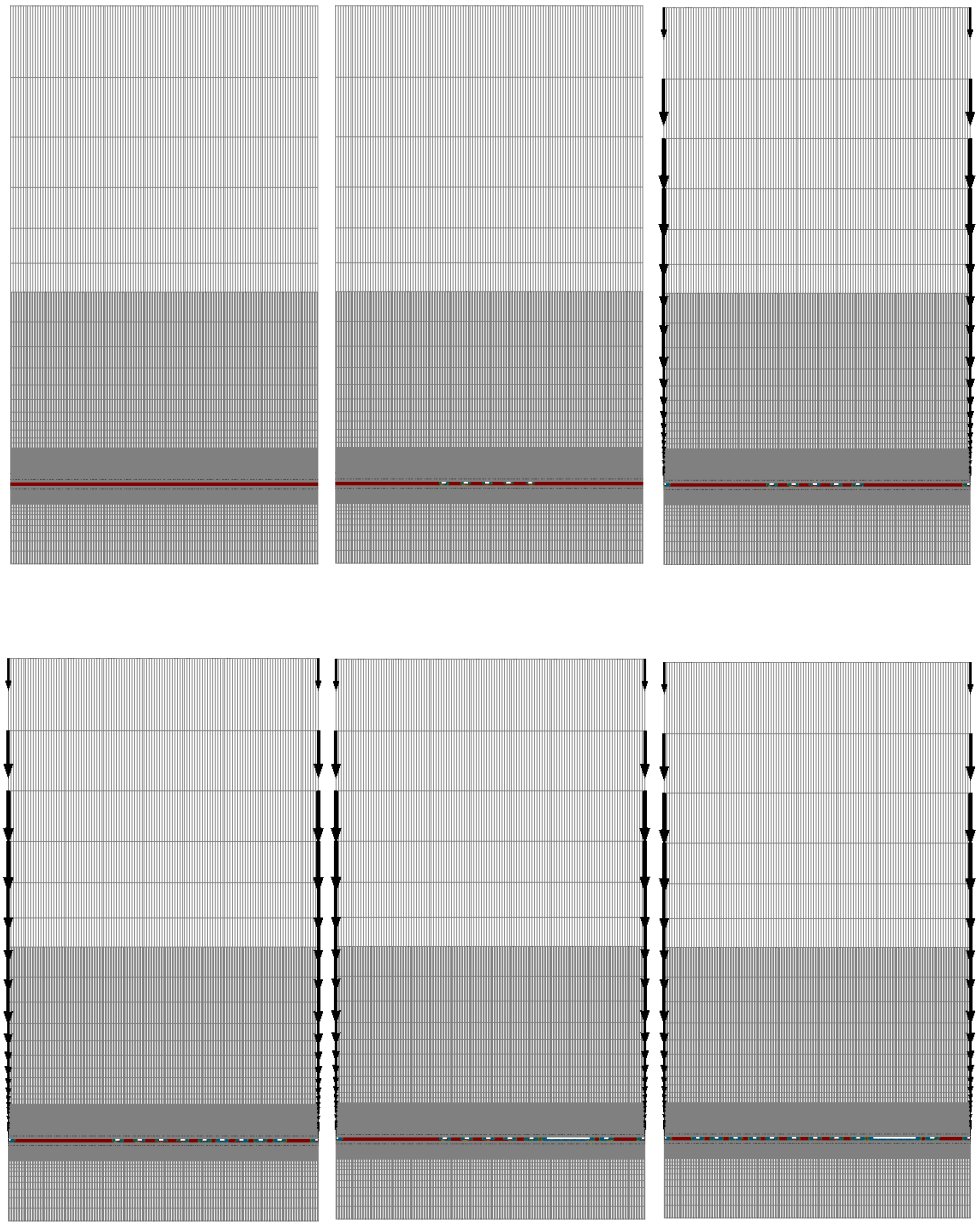

Figure 4.22 Sequence of mining steps as modeled in FLAC3D modeled to represent conditions leading to massive collapse

The complete mining sequence was simulated in the three resulting FLAC3D and nine UDEC mine scale models. Unstable excess energy was calculated in FLAC3D and damped kinetic energy was calculated in UDEC as a measure of the instability experienced at different stages of mining. These magnitudes were used to represent a simulated mine collapse through the brittle material model combinations and to evaluate the influence of varying failure modes of the coal pillars.

4.8.1 Mine modeling results

The results of the quasi-brittle coal models were compared between FLAC3D and UDEC for a fixed coal-rock interface condition. These values are reported in Figure 4.23 in kJ units of excess energy calculated per meter in the in-plane direction. Four stages of mining are reported on namely the development of the Main West section, the development of the North Barrier section into smaller pillars (NBP), the retreat of pillars in the North Barrier section (NBP Retreat), and the development of the South Barrier section into smaller pillars (SBP).

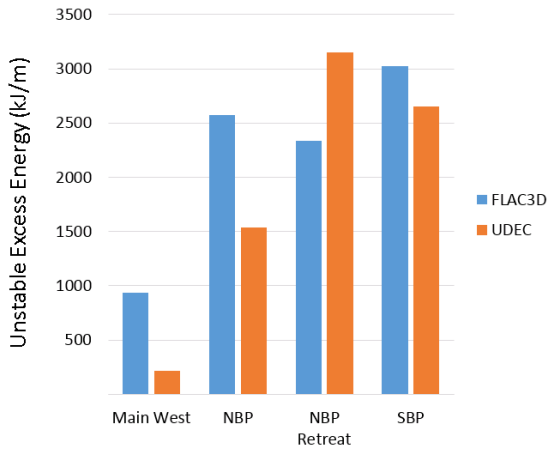

Figure 4.23 Excess energy in FLAC3D and UDEC mine scale MCSS models

The excess energy magnitudes were seen to be much higher in the barrier pillar sections than in development of the Main West entries. This trend is further highlighted in Figure 4.24 where the excess energy is divided by the volume of material removed during each mining stage. This produces the units of kJ/m^3 as a normalized measure of the excess energy release rate per m^3 of mined material. The UDEC results specifically show good agreement to the increased magnitudes of unstable failure which were witnessed as mining progressed.

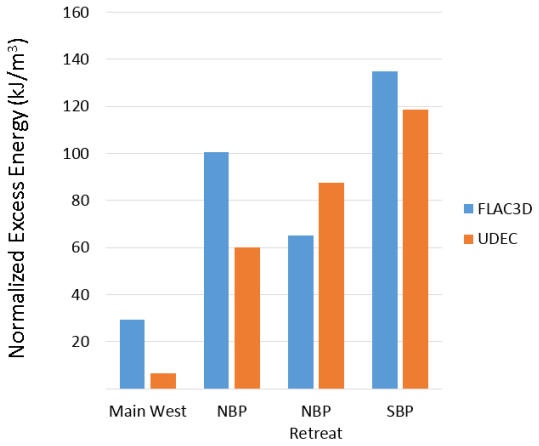

Figure 4.24 Excess energy in FLAC3D and UDEC mine scale MCSS models normalized by the area mined in each stage

The empirical relationship given as $\log E_s = 1.96\, M_L + 2.05\, Joules$ has been used in previous analyses of mine collapses to determine the radiated seismic energy from the local magnitude of the seismic

event (Pechmann et al., 1995). In order to convert our values of unstable excess energy from two-dimensional models into a comparable form as the radiated seismic energy found in this equation, we needed to make an assumption as to the extent of uniform collapse in the East to West direction. Based on a closing crack model proposed by Pechmann et al. (2008), the length of the collapse zone was taken as 920 m in the East-West direction.

From our own calculations of excess energy per meter in the third direction, the equivalent energy was determined for the development stage of the pillars in the South Barrier section with the assumption that a 920 m long section failed in unison. If all of the energy seen during development of the South Barrier section was released suddenly as a single event, then the seismic sources would have the equivalent local magnitudes shown in Table 4.6.

Table 4.6 Projected energy magnitudes of mine scale MCSS models

	Excess Energy [MJ/m]	Total Energy (x920m) [MJ]	Local Magnitude (M_L)
FLAC3D	3.03	2,783	3.77
UDEC	2.65	2,442	3.74

The empirical relationship between radiated seismic energy and local magnitude provides a rough approximation for how well the numerical results match with expected energy magnitudes. Local magnitudes of 3.77 and 3.74 were determined from FLAC3D and UDEC, respectively. These values were contingent upon the additional assumption that all radiated seismic energy during development of the South Barrier section was released as a single event. The representative collapses were seen to be smaller than the 3.9 local magnitude Crandall Canyon collapse due to smaller than expected values for the change in gravitational potential energy and the radiated seismic energy.

The results of excess energy released as a consequence of South Barrier development are shown in Figure 4.25. Once again, the greatest released energy was observed in the MCSS-CY model with increasing magnitudes of energy related to the increasing brittleness of the models.

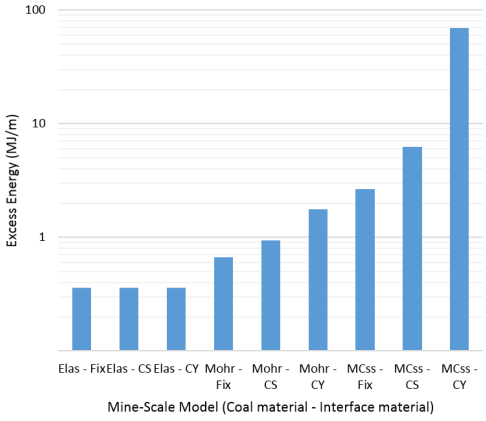

Figure 4.25 Excess energy released during development of South Barrier section in UDEC mine-scale model

Table 4.7 presents the energy values in terms of the total excess energy if the extent of the collapse was assumed to be 920 m in the East-West direction. These estimates of radiated excess energy were then converted into the local magnitudes of the seismic events which they represent. All excess energy during development of the South Barrier section was attributed to a single seismic event. Note that the combinations of elastic and perfectly plastic material combinations cannot result in unstable failure conditions and that the excess energy released in these tests was due to numerical noise introduced through the simulated mining procedure.

Table 4.7 Energy to local magnitude (M_L) conversion for development of South Barrier section

Coal Material	Interface	Excess Energy (SB Dev.) [MJ]	Equivalent M_L
Elastic	Elastic	330	3.3
Elastic	Coulomb slip	332	3.3
Elastic	Continuously-yielding	329	3.3
Mohr-Coulomb	Elastic	612	3.4
Mohr-Coulomb	Coulomb slip	865	3.5
Mohr-Coulomb	Continuously-yielding	1,630	3.7
MCSS	Elastic	2,440	3.7
MCSS	Coulomb slip	5,770	3.9
MCSS	Coulomb slip	2,950*	3.8*
MCSS	Continuously-yielding	63,600	4.5
MCSS	Continuously-yielding	49,860*	4.4*

* - Value was obtained from the formation of the entry with the highest resulting excess energy

The two models of greatest interest were the Mohr-Coulomb strain-softening coal with either Coulomb slip or Continuously-yielding interface properties (see Section 4.9.1 and 4.10 for Continuously-yielding interface model). The magnitudes of these failures represented 3.9 and 4.5 local magnitude events, respectively. The large collapse event which was observed in the MCSS-CY model was further isolated and shown to represent a 4.4 local magnitude seismic event. This can be compared to the much smaller 3.8 event seen in the MCSS-CS model during the formation of the #4 Entry in the South Barrier section. The true local magnitude of the Crandall Canyon was 3.9, however due to numerical noise in the models and the attribution of all excess energy to a single seismic event, it is thought that the Coulomb slip interface led to a lower than expected value of excess energy while the Continuously-yielding interface model produced higher than expected values.

4.9 UDEC modeling with failing rock-coal interface

The UDEC results corresponded well with FLAC3D in the case of a fixed coal-rock interface (Figure 4.23 and 4.24). The UDEC model was then used to evaluate the role of interface effects on the expression of unstable failure at the time of the March 10 bump. The energy results are presented for all other material combinations, but a focus is given to the Mohr-Coulomb strain-softening coal (MCSS) with either a Coulomb-slip (CS) or a Continuously-yielding (CY) pillar contact behavior.

The unstable failure of the Main West section of the mine is reproduced in the two-dimensional distinct element code UDEC and the magnitude of unstable failure is quantified by calculating the kinetic energy released during mining. An overview of the study is given in the following sections, which include the

assumptions and input parameters used in the modeling approach and a discussion of energy calculations.

4.9.1 Interface modeling approach

The model constructed for this analysis is identical to the 2D model described in Section 7. The material above and below the coal seam is modeled as an elastic medium. The continuous overburden forces the system of pillars across the coal seam to work simultaneously against the roof as excavation and loading conditions progress. This approach was adopted because of the presence of stiff overburden units at the mine and the nature of the collapse, in which a large number of pillars failed together (Gates, 2008).

A thorough calibration of material properties was performed before execution of the mine-scale models. In this process, a series of individual pillar models with varying w/h ratios were failed under compression to ensure that their peak or nominal strength was consistent with the predicted strength of similarly-sized coal pillars given by Salamon and Munro (1967) and Mark (1999). These tests were performed with a fixed interface between the coal and rock. The material properties of the coal and overburden used in the mine-scale simulations are shown in Table 4.8 and the Mohr-Coulomb strain softening parameters used for coal are shown in Table 4.9.

Table 4.8 Material properties used in mine-scale simulations

Material	Density (kg/m^3)	Young's Mod. (Pa)	Poisson's Ratio	Friction Angle (deg)	Cohesion (Pa)	Dilation Angle (deg)	Tensile Strength (Pa)
Overburden	2350	23.4e9	0.26	-	-	-	-
Coal	1313	3.0e9	0.20	23.0	1.69e6	2.0	0.0

Table 4.9 Mohr-Coulomb strain softening parameters used in coal

Cohesion (Pa)		Friction Angle (deg)		Dilation angle (deg)	
0.00000	1.69E+06	0.00000	23	0.00000	2
0.00006	1.54E+06	0.00007	27.5	0.00007	10
0.00008	1.47E+06	0.00010	30	0.01360	10
0.03500	2.00E+05	1.00000	30	0.01413	2
1.00000	2.00E+05			1.00000	2

Calibration of interface properties was performed prior to the mine-scale study. A friction angle of 20 degrees and cohesion of zero were selected for the Coulomb Slip (CS) interface. This friction angle lies

within the range of 10 to 25 degrees suggested for fault gouge and smooth rock surfaces respectively (Iannacchione, 1990), and zero cohesion was assigned as a conservative measure. Parameters of a Continuously Yielding (CY) joint were based upon examples provided in the UDEC user's manual and adjusted after running a series of single pillar models with both CS and CY joint properties applied to the coal/rock interface. The single pillar models were compared to ensure that the peak strength of a pillar with one coal/rock interface was comparable to the other. Simple direct-shear test models were also constructed to compare the constitutive behavior of the two joints under identical conditions. The shear stress/displacement graphs for the CS and CY joint constitutive models are shown in Figure 4.6 and the joint parameters are shown in Table 4.10.

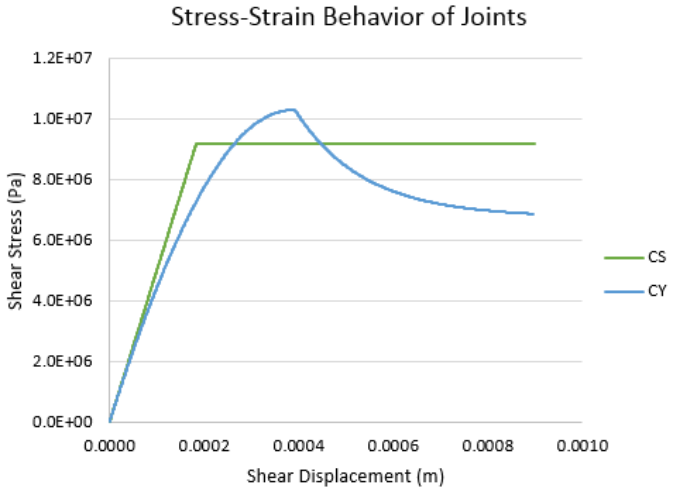

Figure 4.26 Shear stress / shear strain curves of joints used in coal/rock interfaces

Table 4.10. Properties of joints used in coal/rock interfaces

	Coulomb Slip	Continuously Yielding
Shear Stiffness (Pa)	50.0e9	50.0e9
Normal Stiffness (Pa)	50.0e9	50.0e9
Initial Friction angle (deg)	20.0	40.0
Intrinsic Friction angle (deg)	-	15.0
Joint roughness (m)	-	0.00015
Cohesion (Pa)	0.0	-
Dilation angle (deg)	0.0	-
Tensile Strength (Pa)	0.0	-

Numerous direct-shear tests were performed on the CS and CY constitutive models to gain understanding of the shear stress and deformation that is calculated within the software under varying

loading conditions. The observed conditions included velocity-based loading, pressure-based loading, the reversal of shear direction during loading, and the loss of normal confinement during shear loading.

The direct-shear model consisted of two simple blocks, as shown in Figure 4.27. The lower block is fixed on three sides and the upper block is loaded vertically using normal boundary stress. The blocks contain four zones each. In this manner, the number of contacts between the blocks is limited to just two (one at each bottom corner of the upper block) and results could be validated manually.

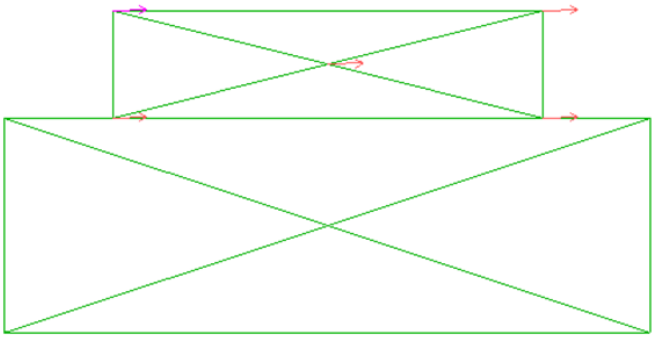

Figure 4.27 Typical direct shear test in UDEC

4.9.2 Excavation sequence

Each mine entry was divided into vertical slices 0.4 meters wide and mined one slice at a time from left to right. Furthermore, each slice was deleted and replaced with equivalent reaction forces, which were reduced over 100 increments to avoid the potential dynamic effects of rapid material removal. This gradual method of excavation was accomplished by using the "Solve Relax" command in UDEC. By excavating as slowly and stably as possible, resultant kinetic energy is attributed directly to changes in the state of static equilibrium throughout the model. On the mine scale, the excavations and abutment loads were developed in the following general order:

1. Excavation of Main-West entries 1 – 5
2. Abutment load on south boundary of model
3. Abutment load on north boundary of model
4. Excavation of entries 1 – 4 in north barrier
5. Retreat mining of two pillars in north barrier
6. Excavation of entries 1 – 4 in south barrier

4.9.3 Energy calculations

UDEC provides an energy calculation procedure and records several energy terms in individual histories. The value of released energy is governed by the following equation:

$$W_r = U_k + W_k + W_v + U_m$$

where

W_r is the total released energy

U_k is current value of kinetic energy in the system
W_k is the total work dissipated by mass damping
W_v is the work done by viscous boundaries
U_m is the total strain energy in excavated material.

This equation was modified to eliminate terms that are not applicable when comparing model results. The work done by viscous boundaries, W_v, is zero because the models in this study do not have viscous boundaries. Additionally, the strain energy of mined material, U_m, was excluded from released energy totals because it represents a magnitude of energy that is subtracted from the system but not released in a sense that is of interest to the study. Thus, the total released energy during the simulation is accounted for by the equation:

$$W_r = U_k + W_k$$

Comparison of W_r values between different mine-scale models provides a scalar measure of the unstable failures that take place, while plots of the changes in kinetic energy indicate when unstable failures occur. A summary of the total energy released, W_r, in all nine mine-scale simulations is shown in Figure 4.28.

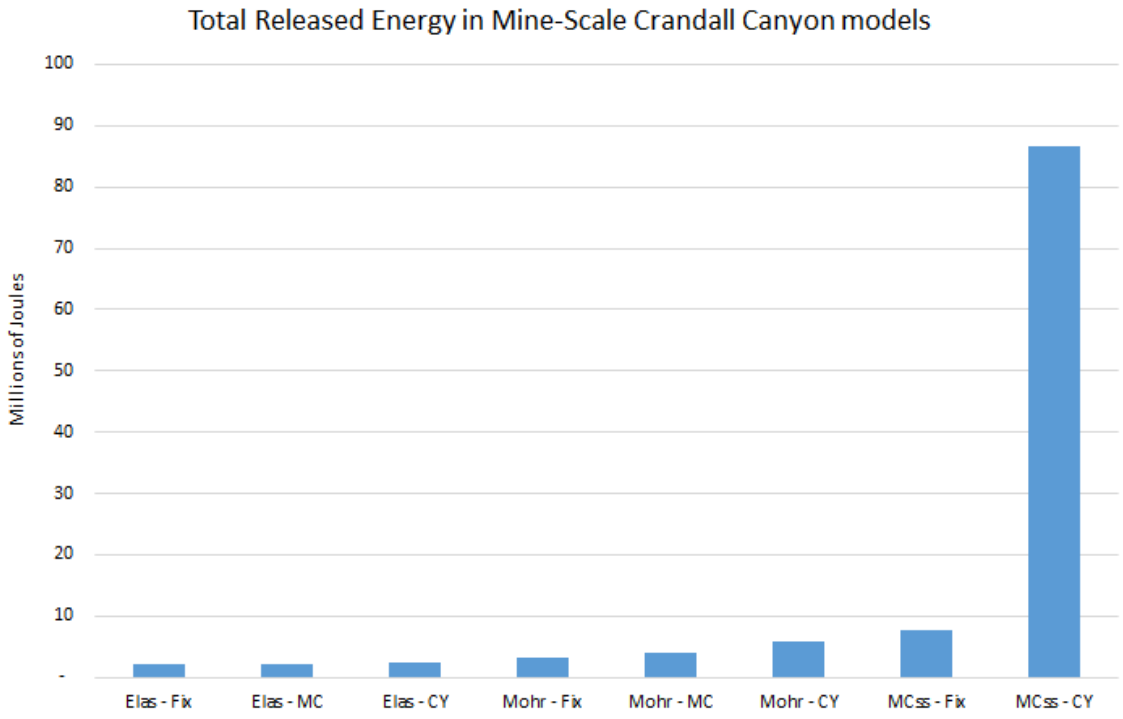

Figure 4.28 Total energy released in all nine mine-scale simulations

Although the mine-scale modeling data files were constructed with the intention of simulating pillar retreat and floor coal removal in the South Barrier, collapse occurred in the MCSS-CY model before

retreat operations had begun. For that reason, results of energy release are shown for each model up to the same stage of excavation, in which four entries are developed in the South Barrier.

It is worth noting that the energy results are for 2D models with an assumed depth of one meter in the third direction. Correlation of 2D results with actual events would require the multiplication of the energy magnitudes by a third dimension in the units of meters.

4.9.4 Failure of a Pillar

This section describes the difference in strength of a pillar from the mine-scale models with either CS or CY coal/rock interface parameters. The MW3 pillar is considered here, which is located near the center of the cross section model shown in Figure 4.19. The behavior of the pillar is compared between two states: 1) when two of four entries have been developed in the North Barrier, and 2) when three of four entries have been developed in the North Barrier.

Figure 4.29 shows stress/strain response of the MW3 pillar before and after excavation of the third entry in the North Barrier. Note that very little increase in stress occurs in the model with the CS interface while development of the third entry produces pillar failure with the CY interface. It is worth noting that the pillar bound by the CS interface exhibits hardening behavior throughout the time period considered in this study, eventually reaching a stress value of 34 MPa.

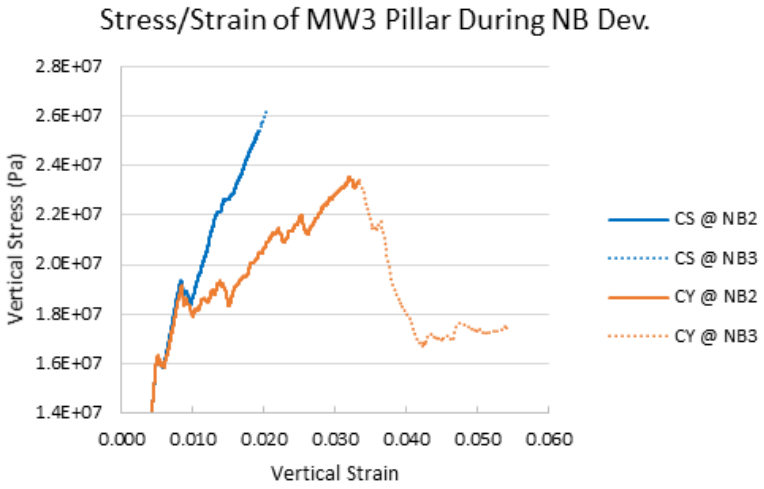

Figure 4.29 Stress/strain of MW3 pillar before and after development of third entry in North Barrier. Results shown for two models with different coal/rock interface properties.

Figure 4.30 shows the distribution of vertical stresses at mid height of the MW3 pillar before and after the third entry is developed. The Coulomb slip interface provides confinement closer to the ribs that allows vertical stress to be sustained across a larger interior portion of the pillar. The CY interface, however, promotes a larger yield zone at the perimeter of the pillar and forces a much higher concentration of stress at the core. These two modes of pillar behavior, dependent upon shear confinement in the coal/rock interface, were conceptualized by Gale (1999) in a study of pillar strength and surrounding strata properties.

Figure 4.30 also shows that the high-stress core of the pillar with the CY interface reduces in width and load-bearing capacity during failure. Successive loading on this pillar will induce softening along portions of the coal/rock interface closer to the core, promoting additional horizontal displacement near the ribs, and further de-confinement and softening of the core. The potential for unstable pillar failure is tied to the stiffness of the loading system, meaning that sudden failure of the pillar will occur if the roof, or a portion of the roof, becomes capable of large sudden displacements.

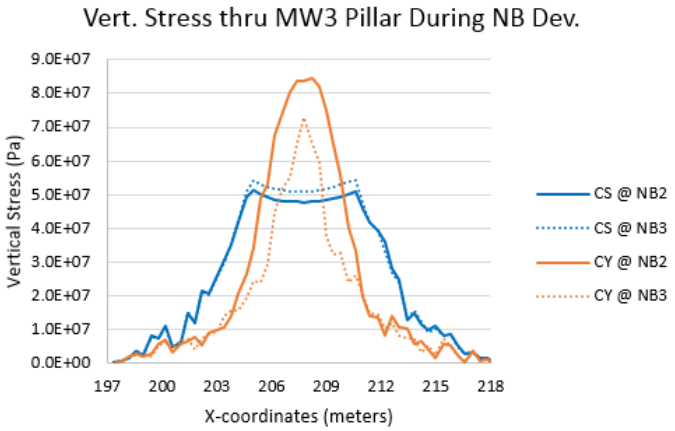

Figure 4.30 Distribution of vertical stress, at different stages of excavation, through pillars with differing coal/rock interface properties

4.10 Kinetic energy release considerations

This section contains results of the mine-scale numerical models for two different phases of mining in the Main West section including: 1) development of the North Barrier with discussion of energy release and pillar deformation, and 2) development of the South Barrier with discussion of energy release and the evidence of a collapse event.

4.10.1 Development of North Barrier

The development of entries in the north barrier reveals a significant difference between the models with CS and CY coal/rock interface properties. Plots of kinetic energy release are shown in Figure 4.31, with results of the CS interface model shown in blue and the CY model shown in orange. The x-axis represents a scale of simulation time, which is a function of the time step used in calculations and the number of time steps that have been executed. This figure shows that the magnitude of kinetic energy spikes is relatively small in the range of tens of thousands of Joules for both the CS and CY interface models. The size of the energy spikes indicates that the softening interface between the coal and rock facilitates individual failure events of greater magnitude.

Figure 4.32 shows the accumulation of released energy throughout development of the North Barrier. The stepped features in the lines indicate small instances of instability, which correspond to spikes of various sizes in the kinetic energy plot. The difference in overall size of the lines illustrates that the softening coal - rock interface results in a significantly greater release of energy.

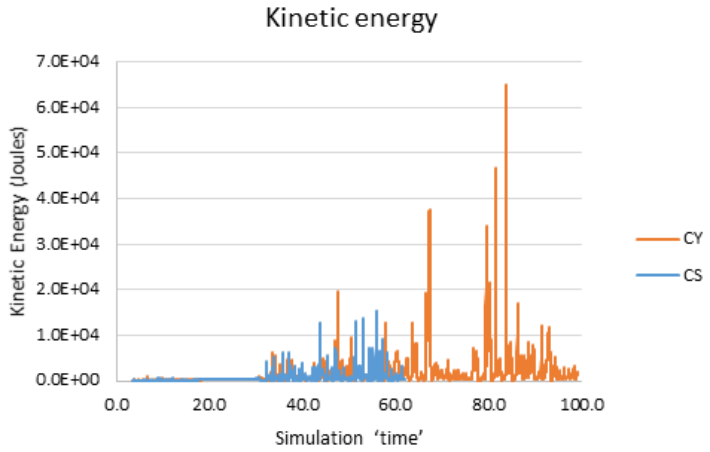

Figure 4.31 Kinetic energy release during development of NB

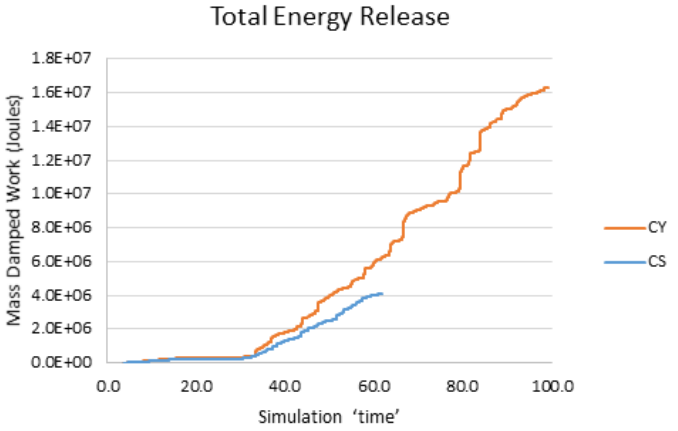

Figure 4.32 Total released energy during development of NB

The difference in pillar response between the two interface models CS and CY is reiterated in Figure 4.33, which shows the stress/strain behavior of the pillar located between the first two north barrier entries, pillar NB1 in Figure 4.19.

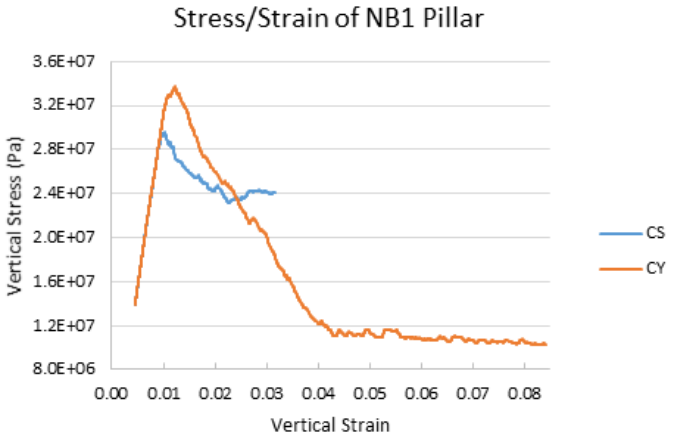

Figure 4.33 Average vertical stress/strain of NB1 pillar

In this area of the mine, the pillars in both models have failed, but the contribution of the coal/rock interface properties is made evident by the higher peak strength and lower residual strength of the CY model. The pillar bound by a Coulomb Slip interface exhibits a higher residual strength, and the smaller value of vertical strain indicates less closure in the coal seam.

4.10.2 Development of South Barrier

Development of the entries in the South Barrier, particularly the fourth entry, results in a massive failure in the model with softening coal/rock interface parameters. The magnitude of this failure is evidenced by spikes in the plot of kinetic energy, shown in Figure 4.34, where the largest spike is in the range of mega joules (MJ).

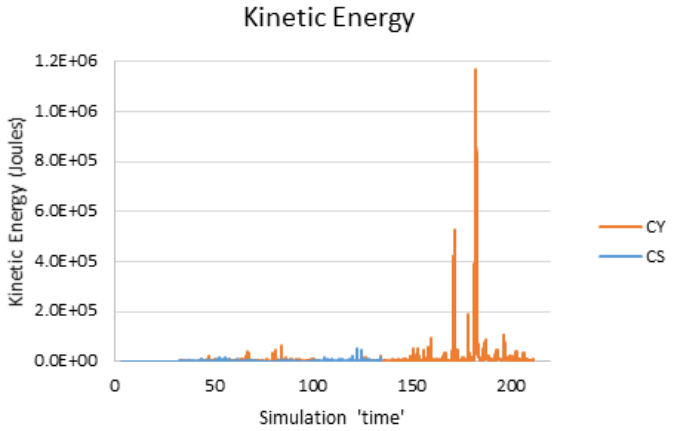

Figure 4.34 Kinetic energy release after development of SB

Figure 4.35 shows the cumulative energy released during all stages of development. The graph illustrates a significantly higher release of energy with the use of the Continuously-Yielding parameters in the coal/rock interface, and the large stepped portions of the curve correspond to the magnitude of energy associated with widespread failure.

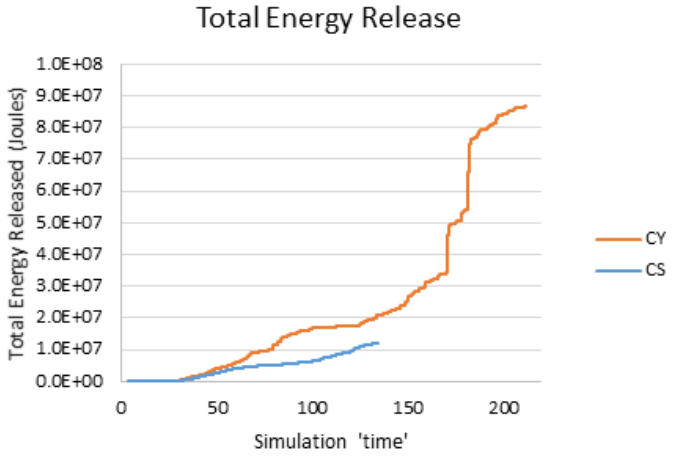

Figure 4.35 Total released energy during development of SB

The energy of the collapse is illustrated in Figure 4.36 with the values of energy released per stage of development in both the North and South Barrier. The graph shows that development of the final entry resulted in the release of approximately 54 MJ with the softening coal/rock interface. The amount of energy released during development of the same entry in the simulation with a CS interface was only 3.2 MJ, signifying a much lesser degree of unstable failure in the coal seam and more than an order of magnitude difference in released energy between the models. Although there was no evidence of widespread pillar failure in the model with the Coulomb slip interface, the development of the final entry still accounted for a significant portion of the released energy in that simulation.

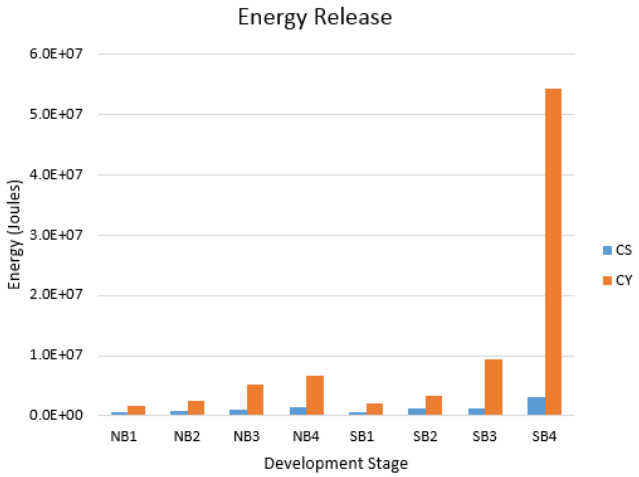

Figure 4.36 Energy released during each stage of development in NB and SB

4.10.3 Roof displacements from pillar failures

Indication of the large failure event is further supported by the roof displacement contours shown in Figure 4.37. The graph illustrates the extent of closure in each model before and after development of the four South Barrier entries. Additionally, the graph contains a closure scanline for the state of the CY model in which only three of the last four entries are developed, referred to as SB3. The SB3 line helps illustrate the closure that occurred during development of the final entry. The configuration of pillars and entries present in the final state of the model is shown in the diagram near the top of the graph.

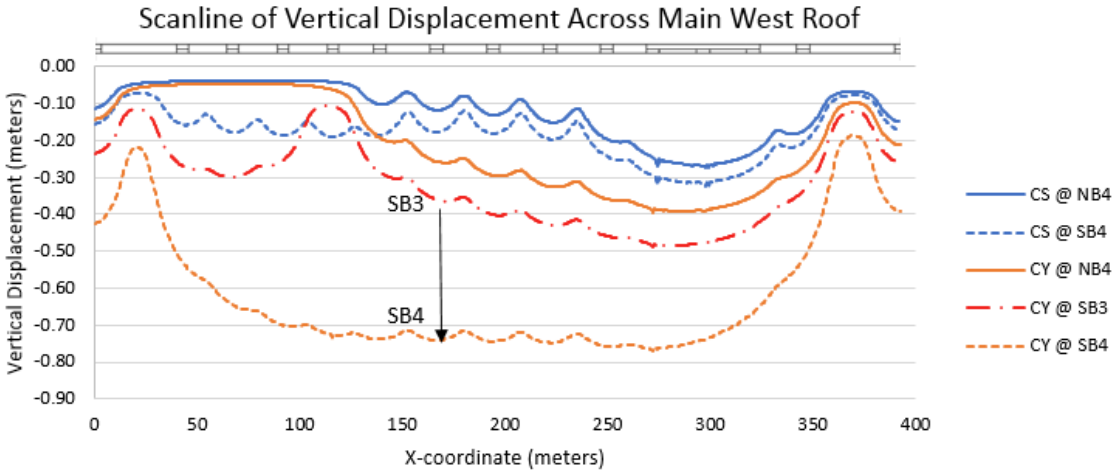

Figure 4.37 Closure scanlines before and after development of the South Barrier entries

The unstable failure of pillars in the CY model between stages SB3 and SB4 is supported by the displacements in Figure 4.37 and the energy released in Figure 4.36. Development of the SB4 entry subjects the system of pillars across the Main West to loads beyond their collective strength, and the stiff overburden moves downward until resistance is re-established by the remnant barrier pillars in the north and south. The unstable failure of the pillars is attributed to the softening characteristics of the coal and the coal/rock interface as well as the "softness" of the loading system, which refers to the downward displacement of the overburden without obstruction.

4.11 General Chemical case

Three roof collapses occurred in 2000 within the General Chemical trona mine in the Wyoming Green River Basin. These collapses were located within active retreat panels as the extraction ratio reached 87%. The failures were restricted to rectangular collapse areas measuring roughly 175 m on a side (see Figure 4.38). In each case, the collapse was attributed to undersized pillars leading to failure in the roof. Notably, no surface subsidence was observed following these collapses as it was thought that the failure was terminated by a very strong sandstone unit located approximately 100 m above the active seam (Board and Damjanac, 2007).

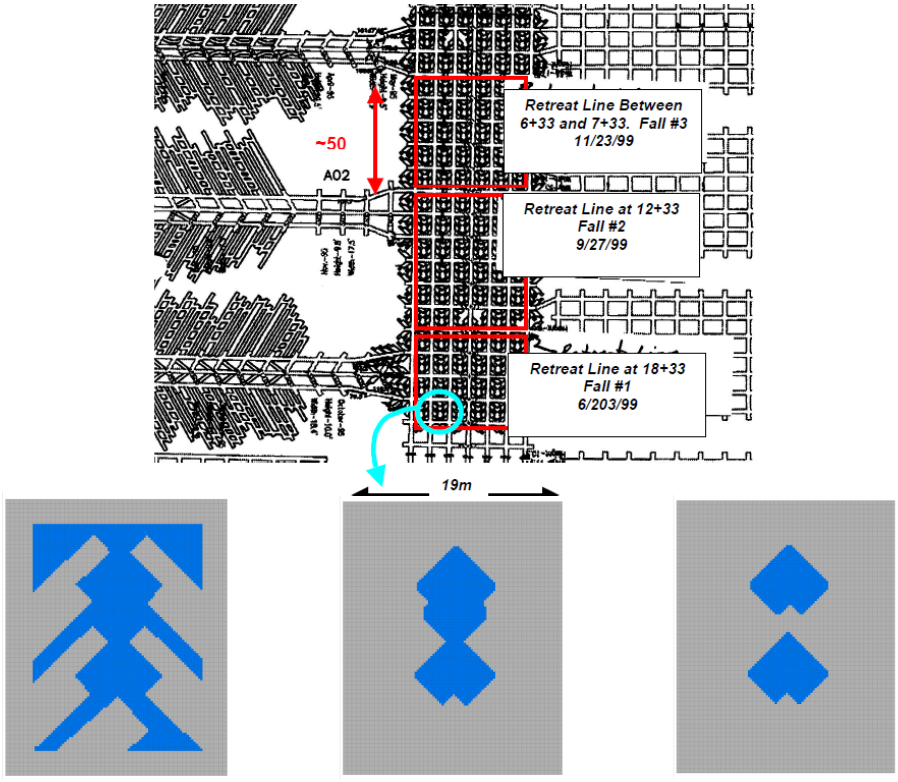

Figure 4. 38 Map of the three collapsed areas (top) and Plan view of trona pillars (blue) developed during retreat mining. Progression shows a) 67% extraction, b) 87% extraction, and c) an assumed 89% extraction (from Board and Damjanac, 2007).

The retreat mining stages reduced pillar geometries into the shapes as shown in Figure 4.36 below the mine map in Figure 4.38. The initial extraction ratio was approximately 67% and was increased to 87%. In some cases, damage to the pillars led to an extraction ratio closer to 89%.

Instrumentation in the mine and numerical modeling conducted by previous researchers (Board and Damjanac, 2007) provided an average stress-strain behavior for the pillars at each level of extraction. This stress-strain behavior is given in Figure 4.39 in the form of average "backpressure" applied to the roof exerted onto the area of roof supported by the pillars.

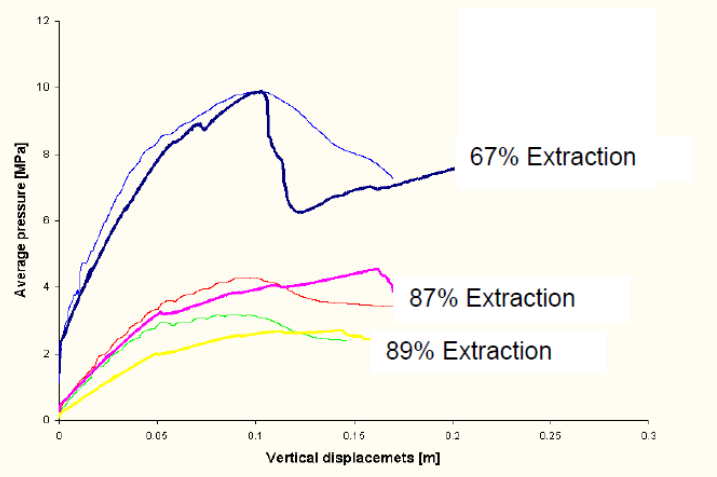

Figure 4.39 Numerically-derived support curves for trona pillars in General Chemical mine (from Board and Damjanac, 2007). Given in terms of backpressure applied to the area of support, with thick lines representing 2D results.

Due to the slender nature of the pillars at 87% extraction, the support behavior may be reduced to purely vertical tractions with little effect coming from horizontal forces at the pillar contacts. This simplification of support behavior greatly reduced the modeling effort needed to effectively capture the force-displacement characteristics of pillars at seam level.

4.11.1 General Chemical models

4.11.1.1 Model description

Focusing on the energy release considerations from the three unstable failures at the mine, we re-constructed a two-dimensional FLAC3D model of a 175 m wide mining span within a rockmass with strength properties provided by Board and Damjanac (2007). A plane-strain condition with half symmetry was taken to reduce computational requirements (Figure 4.40). Pillars were modeled using vertical forces applied along the roof and the floor. The magnitudes of these forces varied according to the vertical closure of the seam in order to model a changing backpressure provided by quasi-brittle pillars. A complete program listing of the files used to generate these tests may be found in Appendix III, with the file 'general_chemical_batch_v21_pressure.f3dat' providing a means of running the complete series of tests in FLAC3D v5.0.

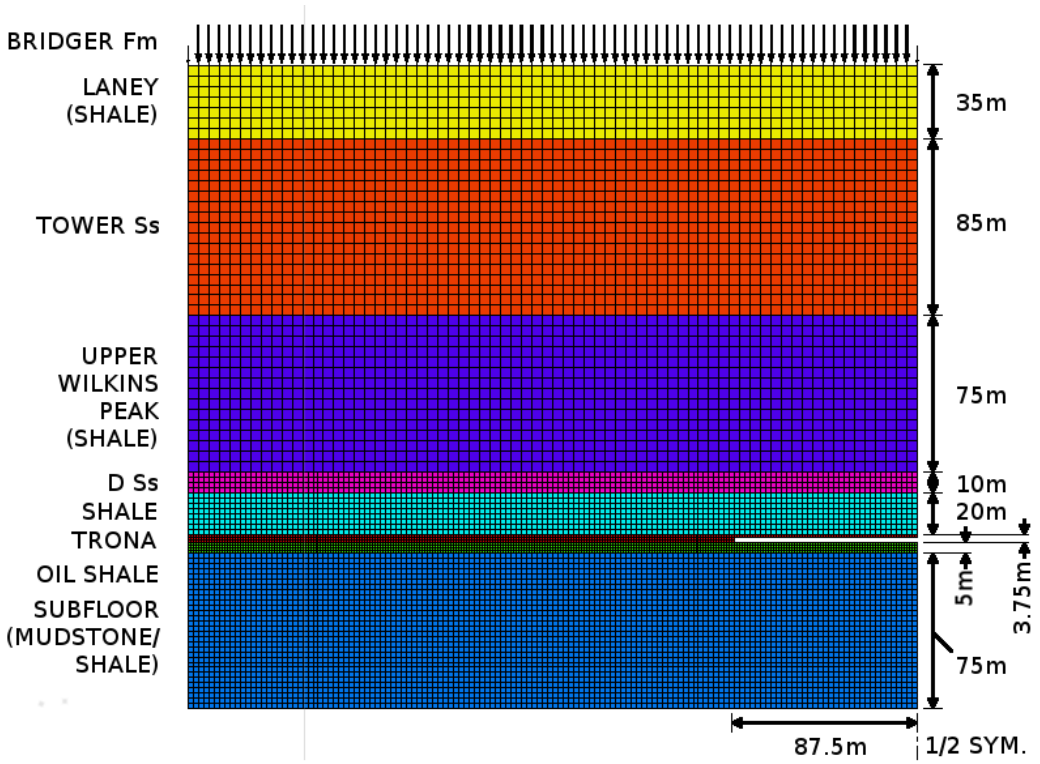

Figure 4.40 FLAC3D model of General Chemical span and rockmass

An extraction ratio of 87% was assumed for the mining span. Forces were applied to gridpoints such that the vertical pressure on the face of the attached zones was equal to the desired backpressure. The post-failure support backpressure was modified to include the four possibilities shown in Figure 4.41. Changes in this behavior led to either more or less energy being consumed by the supports during failure, with the ductile Variant 3 absorbing the most energy of the options shown.

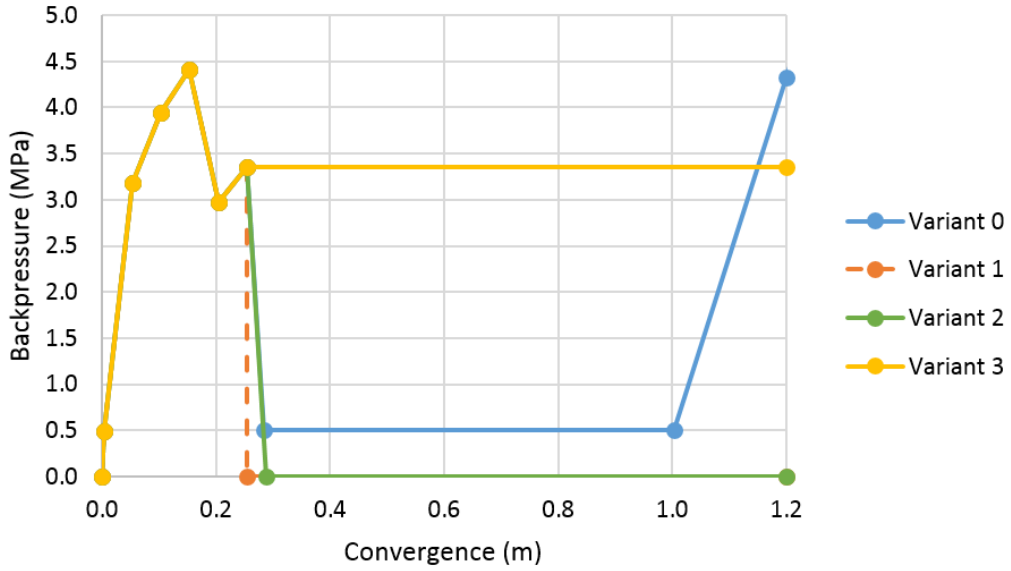

Figure 4.41 – Variations of support pressure used to represent 87% extraction ratio

The strengths of the overburden strata were taken from ranges provided by Board and Damjanac (2007) and were calibrated further so that failure was initiated a retreat span of 175 m and an average seam closure of 0.25 m. A complete listing of the calibrated model inputs is provided in Table 4.9.

Table 4.11 FLAC3D inputs of rockmass properties in General Chemical study

Unit Label	Thickness (m)	Density (kg/m^3)	Young Mod. (GPa)	Poisson ratio	Friction (deg.)	Cohesion (MPa)	Dilation (deg.)
Bridger (poorly consolidated)	240 to 265	2250	0 (Pressure)				
Laney Shale	35	2250	6	0.26			
Tower Sandstone	85	2250	26	0.2	40 to 44	8.6	10
Upper Wilkins Shale	75	2250	10	0.26	28	1.4	10
D Sandstone	10	2250	26	0.2	32 to 36	5 to 0	10
Roof Shale	20	2250	10	0.26	25	1.6	10
Trona	3.75	2250	28	0.4	36	2.9	10
Oil Shale	5	2250	4	0.26			
Mudstone	75	2250	6	0.26			

A Mohr-Coulomb constitutive law was applied to the shale units above and below the stiff D Sandstone. The D Sandstone was taken as a Mohr-Coulomb strain-softening material, however the effects due to brittleness of the sandstone were investigated as will be discussed further in this report. Variations to the cohesion of the D Sandstone are provided in Figure 4.42 as functions of plastic strain. The file 'general_chemical_batch_v21.f3dat' found in Appendix III was used to conduct this series of tests.

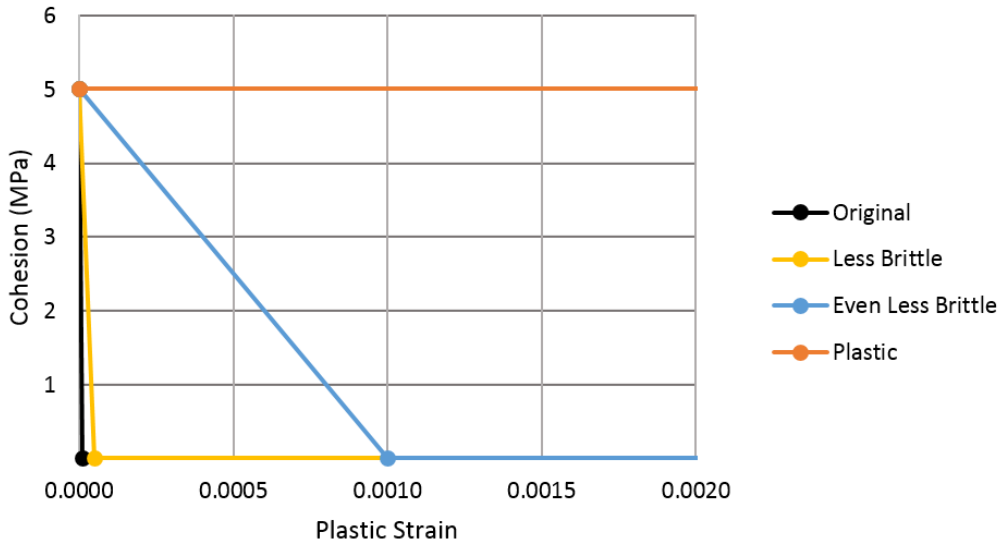

Figure 4.42 – Variations of cohesive strength applied to the D Sandstone stratum in roof

4.11.1.2 Energy calculations

The model was first loaded only by gravity. Pressures were then applied to the top of the model to represent the approximately 240m of poorly-consolidated sedimentary units above the Laney Shale unit. These pressures were increased slowly to not introduce dynamic effects into the model thus not significantly affecting the excess energy calculations. Quasi-static energy terms were calculated while pressures were added to the top of the model. These terms, listed in Table 8.2, were combined in the form

$$E_u = (W_b + W_t + W_i) - \left(U_c + W_p\right) \quad (unstable\ failure\ if\ E_u > 0)$$

Table 4.12 Energy Components during Mining

W_b: External boundary work
W_t: Body work or the change in gravitational potential energy
W_i: Internal boundary work
U_c: Elastic strain energy in rock
W_p: Work done by plastic deformation of rock
E_u: Unstable excess energy

The external boundary work was the work done by the upper pressure boundary while internal boundary work was the work done by the backpressures applied onto the roof and the floor of the mined span.

When the dynamic effects due to loading were reduced, the remaining unstable excess energy was attributed to the development of unstable equilibria within the rockmass system. These instabilities were produced by the application of a sufficiently soft loading system onto a support system which could neither support these loads nor consume their associated release of energy through plastic deformations. The excess energy was then taken as a measure of the magnitude and degree of the unstable failures which occurred in the models.

4.12 General Chemical results

Parametric simulations were run using the variations of material properties found in the previous section. Collapse events were reproduced for spans of 175m and 200m, while no collapse was observed for any of the combinations used for support behavior and D Sandstone properties at a 150 m span. Each collapse event was identified by a sudden increase in excess energy and a rapid convergence at coal seam level. In each case the much thicker Tower Sandstone stratum in the overburden remained un-failed, thereby limiting the subsidence at the top of the model.

The general collapse process took the form shown in Figure 4.43 before failure and in Figure 4.44 after failure. Large regions of zones in the shale units above and below the D Sandstone were seen to reach their strengths prior to failure of the D Sandstone. When the D Sandstone failed, additional loads were applied onto the supports at seam level, leading to their weakening and a progressive failure mode. The

failure of the D Sandstone and the reduction in support strength were integrally linked such that an analysis of energy terms was required to fully explain the complex interactions which took place within the system.

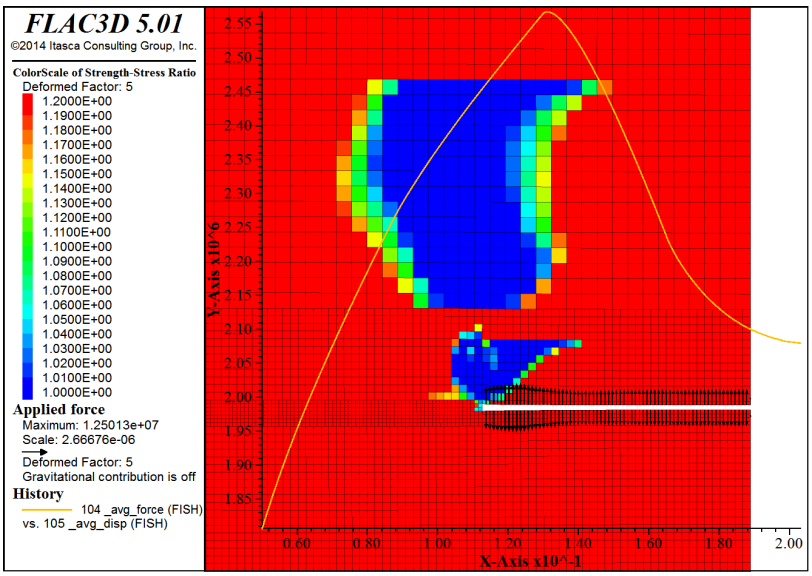

Figure 4.43 – Color contouring showing zones at or near their strength limit. Extensive failure occurred in the shale units above and below the D Sandstone prior to collapse. Support curve at seam level is also plotted and shows the supports are in their residual strength behavior.

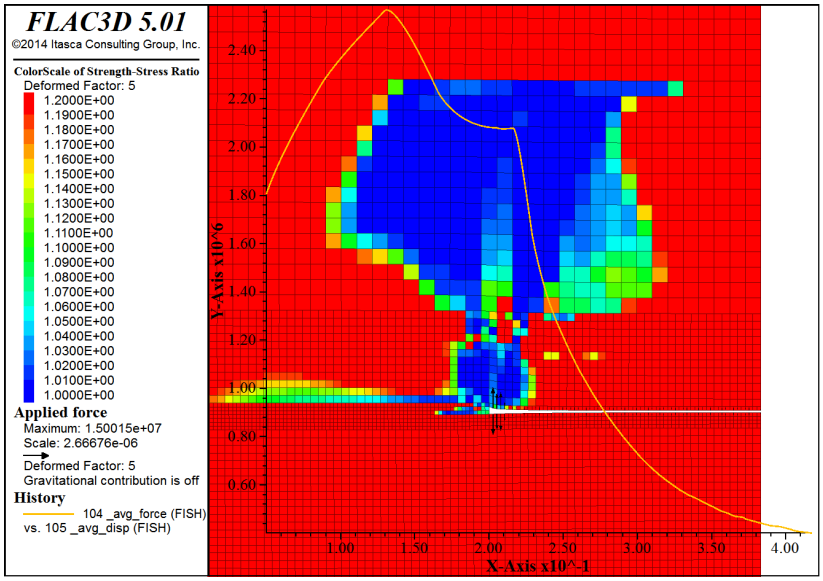

Figure 4.44 – Screenshot after collapse, showing extensive failure of D Sandstone and continued failure of shale units. Little backpressure is provided by the supports at this point.

4.12.1 Energy calculations

The excess energy calculated from each combination of support type and mining span is provided in Figure 4.45. The simulations were stopped when 1.2 m of total convergence had been reached such that energy results could be compared between different support types. These results followed the expected trends of greater energy release in the case of a wider span or a more brittle support behavior. The top pressure which was required to produce a collapse event was different for each combination of model properties. In the case of a 175 m span, this pressure was roughly 5.5 MPa, corresponding to a simulated thickness of approximately 250 m for the Bridger unconsolidated sedimentary units if a density of 2250 kg/m^3 was assumed. Collapse was initiated much sooner for the 200 m span with a top pressure of roughly 4.7 MPa, or a simulated Bridger thickness of 215 m. Continued convergences were observed in the cases of a perfectly plastic support curve (Variant 3), however these collapses did not correspond with an increase in the excess energy due to the capability of the support pressure to absorb the release of energy generated by downward displacements of the roof.

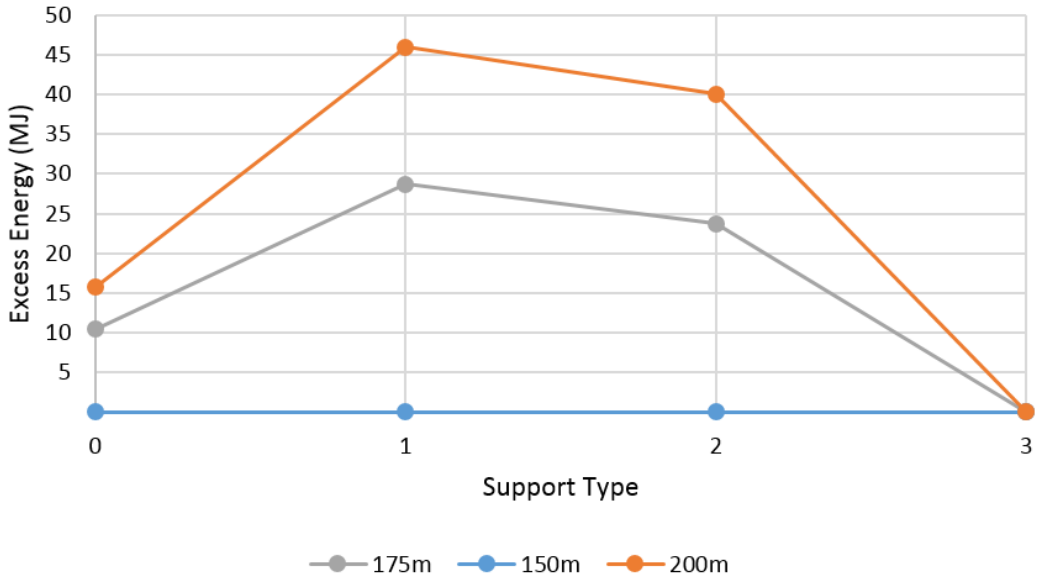

Figure 4.45 Excess energy calculated for the four variations of backpressure support curves at three different spans. Note that collapse was not observed in the case of a 150 m span.

The energy terms in Figure 4.45 are given for the entire FLAC3D models. These models maintained a 1 m thickness, so the energy terms may be thought of the excess energy generated for the half-span per meter of mining in the third direction. The two-dimensional nature of the models does not provide a perfect analogue to the true collapse cases observed in the General Chemical mine. However, a rough approximation of the energy which would be released by these simulated collapse events can be made by assuming an extent of failure in the third direction. The total excess energy values for the models with a 175 m span are given in Table 4.12 for each combination of model inputs.

The length in the third direction was assumed to be 175 m to correspond with the approximate areas of collapse which were reported from the General Chemical mine. Note that this approach will produce an overestimated magnitude of excess energy if breakage of the overburden is less than vertical in the third

direction and the calculation will not take into account plastic energy consumed due to failure of the overburden along these planes. Perhaps a more appropriate method of converting these terms into relatable energy units is to make an axisymmetric assumption of the failure to represent a cylindrical failure plug during collapse. The total values of excess energy are provided in Table 4.12 for both of these assumed shapes of failure in the roof.

Table 4.12 Excess energy from FLAC3D models with 175 m span extended into third dimension

Support Type	Half-Span Excess Energy [MJ/m]	Total Excess Energy (square plug) [GJ]	Total Excess Energy (cylindrical plug) [GJ]
0	10.5	3.7	2.9
1	28.7	10.1	7.9
2	23.8	8.3	6.5
3	0.0	-	-

The modeled results followed expected trends for the given support types and span widths. A question was raised during this study as to whether the excess energy released from the models was produced due to the brittle response of the supports or due to the reduced strength of the D Sandstone following failure. The effect of brittleness was further explored by applying the cohesion tables in Figure 4.42 to the Mohr-Coulomb strain-softening model used to determine strength of the D Sandstone as functions of plastic strain. The results of these models are given in Figure 4.46 below.

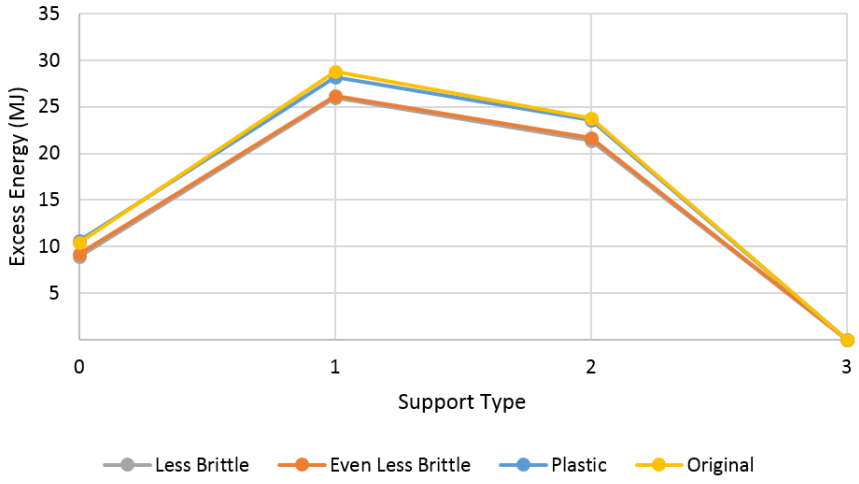

Figure 4.46 – Excess Energy calculation using support curve '0' and testing variations of brittleness in D Sandstone at a 175 m mining span. Note that energy values did not vary significantly as a function of the brittleness of the D Sandstone.

The most striking result of this series of tests was that the excess energy produced by a perfectly plastic D Sandstone unit was virtually identical to the case of a perfectly brittle material response. These results support the conjecture that the collapse was generated by the roof strata being close to failure while the trona pillars were already within the weakening portion of their stress-strain response. A brittle response of the D Sandstone was not required to explain the unstable failures observed within the models

4.12.2 General Chemical results in context of radiated energy and seismic magnitude

The term unstable excess energy is used here to describe the released energy as a consequence of unstable equilibria developing in underground mines. This energy is equivalent to the radiated seismic energy in the case of sudden fault slip or mine collapses. Several assumptions are necessary in deriving the energy radiated from a seismic event; however converting the known energy into a local magnitude offers an intuitive approach in numerical analyses. The following section explores the energy release from simulated collapses to study the effect of support failure behavior on the energy release from unstable systems.

The total excess energy released from a collapse mode relies on the change in potential energy of the overburden and the energy that could be consumed in a stable manner by deformation of the supports. Multiple support behaviors were considered to illustrate the effect of changes to the post-failure behavior on support systems. These additional support types are listed in Figure 4.47. These curves are extensions of 'Variant 0' used in the previous tests but with different residual strengths.

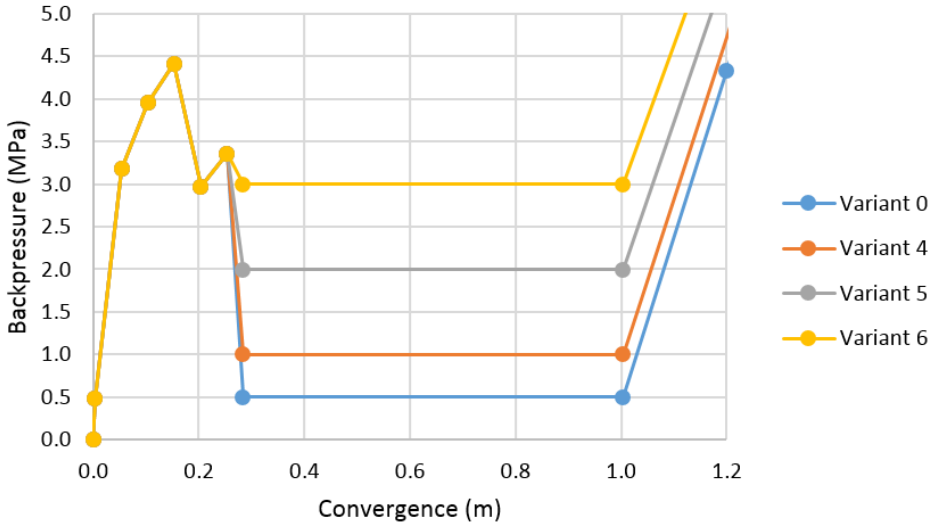

Figure 4.47 – Additional variations of support pressure used to represent 87% extraction ratio in the analysis of radiated seismic energy

The energy results from each test are provided in Table 4.13. These values were derived in an identical fashion as the energy results listed in Table 4.12 where the total energy is calculated based on both a linear extension into the third direction and using the assumption of an axisymmetric failure of the roof. The symbol M_L in the table represents "local magnitude" of a seismic event given by Kanamori et al (1993) in the form

$$\log E_s = 1.96\, M_L + 2.05\ [Joules]$$

which was originally developed from a database of earthquakes and used by the researchers in the mine seismicity field.

Table 4.13 – Excess energy from FLAC3D models with additional support curves

Support Type	Half-Span Excess Energy [MJ/m]	Total Excess Energy (square plug) [GJ]	M_L (square)	Total Excess Energy (cylindrical plug) [GJ]	M_L (cylindrical)
0	10.5	3.7	3.8	2.9	3.8
4	6.0	2.1	3.7	1.6	3.7
5	1.5	0.53	3.4	0.41	3.4
6	0.3	0.11	3.1	0.082	3.0

The variations of post-failure support behavior corresponded to equivalent local magnitudes (M_L) ranging from 3.0 to 3.8. Numerous assumptions were made in these calculations, however given enough information it is feasible to convert energy results obtained via numerical model to radiated seismic energy determined from a seismic analysis and vice versa. A more detailed seismic analysis is required of the General Chemical collapses in order to bring more clarity to these comparisons.

5. Summary of accomplishments

The major technical accomplishment of this project is the development of new modeling methodologies for the analyses and assessments of potential rock burst conditions in highly stressed underground mines. The modeling efforts reveal a new understanding of squat pillar behavior that they may fail thoroughly through shear failure along rock-coal interfaces. Additional significant technical accomplishment is the advancement of energy calculations methods in numerical models that can be further developed toward estimating seismic event magnitudes of rock burst events. These efforts place the status in understanding and combatting rock burst phenomenon ahead of where it was before the start of this project.

The back-analysis of the Crandall Canyon mine collapse provides an opportunity to evaluate the effects of coal material and coal/rock interface properties on unstable failure. Results of this study reveal that the combination of a strain-softening coal material and a shear-softening coal/rock interface facilitates a progression of pillar failure and sudden collapse in the mine-scale model that correlates with the failure events at the mine. Importantly, the collapse in the numerical model indicates that the unstable failure of large width-to-height ratio pillars can be simulated while using commonly accepted input parameters. The UDEC brittle coal models with either a Coulomb slip or a Continuously-Yielding contact condition at the rock-coal interface were seen to closely approximate the estimated closures and radiated seismic energy of the August 6, 2007 collapse. Large collapse events were identified in these models during the simulated development of the South Barrier section. Excess energy values from these collapse events corresponded to local event magnitudes (M_L) of 3.8 in the case of the MCSS-CS model and 5.4 for the

MCSS-CY model. These results were obtained by assuming that the failure occurred uniformly across the approximate length of 920 m of the collapsed portion of the mine.

The General Chemical collapse was straightforward to replicate using support stress-strain behavior provided by previous researchers (Board and Damjanac, 2007) and material properties of the rockmass selected from accepted ranges. Failure of the pillars and continued downward displacements of the calibrated overburden were seen to occur when the panel width was equal to or greater than 175m. Excess energy magnitudes increased with the width of the span which was being modeled. The values of excess energy were reduced when support backpressures were assumed to have a more ductile response. The simulated collapse events could be thought of as a combined failure of the overburden strata and weakening of the supports. A perfectly plastic support curve, while capable of generating a collapse, produced no excess energy as potential energy was removed from the system through a controlled convergence. A perfectly plastic D Sandstone was, however, able to produce a violent collapse when a brittle behavior was assumed for the supports.

The modeling approach demonstrated one method to simulate unstable collapse of a given mining span. The calibration of material properties came from observations made in the mines before and after the collapse. The support behavior was reduced down to a standard backpressure which could be applied directly to the roof and the floor in the form of gridpoint forces. This simplification ignored effects due to progressive failure and loss of confinement in the pillars, however provided a direct method for defining specific support behavior in terms of vertical closure.

Additional significant accomplishment includes the educational outcomes which involve full participation of three PhD students, one research associate, and one post-doctoral fellow, who were actively involved in the development of the new failure stability concepts as part of their thesis or academic research work. The researchers involved in this study all benefited from the opportunities to advance their knowledge in rock mechanics and appreciation of rock mechanics safety in mines. Through their efforts, several technical reports were prepared and papers were published in relevant symposia and conferences.

6. Dissemination efforts and highlights

The research team submitted and presented papers at respectable mining and rock mechanics conferences. Two papers were published at ICGM conference 2014 and 15, another two were presented at 2015 ARMA conference. One of the papers published at the ICGMM conferences was selected by the conference committee to be presented at the next SME meeting in 2016.

Several online and in person meetings were held with NIOSH scientists from the Pittsburgh and Spokane branches on various occasions to receive input and discuss project progress and outcomes. The project was also discussed with mining engineers and scientists from MSHA and NIOSH at conference settings.

The following papers were developed and presented at the International Conference on Ground Control in Mining (ICGCM) and American Rock Mechanics Association (ARMA):

R. Gu and U. Ozbay. (2014) Analysis of deconfinement mechanisms of unstable failures in underground mining conditions. 33rd International Conference on Ground Control in Mining. Morgantown, West Virginia.

Poeck, E., Zhang, K., Garvey, R., and Ozbay, U. (2015). Contribution of shear slip in a widespread compressive pillar failure. The 49th US Rock Mechanics / Geomechanics Symposium, San Francisco, CA, USA.

Zhang, K., Poeck, E. Garvey, R. and Ozbay, U. (2015) Effect of Coal-Rock Interface Properties on Failure Stability of Coal Pillars Expressed in Energy Terms. The 49th US Rock Mechanics / Geomechanics Symposium, San Francisco, CA, USA.

Poeck, E., Zhang, K., Garvey, R., and Ozbay, U. (2015). Energy concepts in the analysis of unstable coal pillar failure. 34rd International Conference on Ground Control in Mining. Morgantown, West Virginia.

Copies of these papers are included in Appendix V.

7. Conclusion and impact assessment

This project focused on assessing unstable failure mechanisms in highly stressed underground mines using explicit numerical methods. The failure mechanisms which were studied within the models yielded similar outcomes as the failures selected from the literature. Consideration of kinetic energy released during controlled excavation steps helps identify unstable failure events while the total released energy provides a quantitative assessment of their magnitude. These methodologies can now be used for mechanistic analysis of unstable failures as well as in the initial assessment of mine layouts for their potential to lead to rock burst events.

Rationally based methodologies are developed for performing backanalysis studies. The backanalysis cases demonstrate the usefulness of an energy-based approach towards identifying and quantifying the emergence of unstable failure conditions in representative mining environments. A great deal of additional knowledge is gained by studying these complex systems in terms of the energy released as a consequence of unstable failure. The methods we developed for calculating excess energies may now be applied with greater confidence to explicit numerical methods using either dynamic or quasi-static energy balances. An appropriate calibration of material properties will continue to be difficult when using this approach; however parametric studies may be conducted over ranges of likely material responses to assess the relative degree of instability for each scenario. Future studies can be performed using these methodologies for assessing rock burst potential in deep mines.

Explicit numerical models used in this study have proved capable of realistically simulating the conditions leading up to unstable failures of brittle rocks and discontinuities. Parametric studies which address the uncertainties in geomechanical systems provides a useful method for capturing ranges of potential outcomes while assessing the effects of various geological and material combinations. Calculations of fundamental energy terms provide a direct and rational approach for understanding the evolving response of these highly complex scenarios. These energy terms may further be used to

correlate observations made in the case of mine failures to the results of numerical models. This research effort has highlighted the significant benefits of incorporating these energy calculations into numerical investigations of coal bump and rockburst phenomena.

The calculations of excess energy which were developed for this project provided a robust method of studying unstable failures as they developed within brittle rock systems. These excess energy magnitudes correspond with radiated seismic energy and may be used to assess the relative magnitudes of simulated seismic events. The approach may be used to study highly complex failure mechanisms where traditional methods of analysis become too difficult to apply.

The repeated application of this numerical assessment to backanalysis cases will provide confidence for these tools to be applied in future mine design. We have already seen significant interest by researchers and mine planners in the calculation of excess energy for evaluating different mining layouts for a given set of rockmass conditions. Such improvements may lead to a better understanding of the risks posed by rock bursts in deep mines.

8. Recommendation for future work

In the case of the Crandall Canyon mine collapse, observational evidence collected at the site is strongly supportive of a shear slip mechanism at the pillar contacts. By incorporating slip at the coal-rock interface, the behavior of large width-to-height ratio coal pillars was seen to match expected pillar strength values while also allowing for extensive failure at the onset of instability. This combination of realistic strength behavior for the coal and for the pillar contacts revealed a mode of failure which was conducive to large releases of excess energy following the onset of unstable equilibria. The potential role of shear slip should be evaluated in future studies of coal bumps in wide coal structures.

This study provided a basic foundation for modeling rock bursts and for studying the effects of induced seismicity in mines. Additional work may be done on developing more realistic constitutive models to represent quasi-brittle rock failing under dynamic loads. This could improve the calculation of the energy consumed through plastic deformations during instability. Further studies on additional mine settings would also give greater confidence to the selection of material properties in failure stability analyses.

9. References

Board, M, B., Damjanac and M. Pierce (2007). Development of a methodology for analysis of instability in room and pillar mines. In Deep Mining 07, Proceedings of the Fourth International Seminar on Deep and High Stress Mining, Yves Potvin (ed),: 273-282.

Cook, NGW (1965) A note on rockburst considered as a problem of instability. Journal of the South African Institute of Mining and Metallurgy, 437-46.

Cook, NGW (1967) The design of underground excavations. Failure and Breakage of Rock – Eighth Symposium on Rock Mechanics 1967;167-93.

Das, M.N. (1986) Influence of width/height ratio on post-failure behavior of coal. International Journal of Mining and Geological Engineering, 4(1), 79-87.

Duvall W. I., Stephenson D. E. (1965) Seismic energy available from rockbursts and underground explosions. Trans AIME 232(3):235-40.

Ford, S. R., D. S. Dreger, and W. R. Walter. (2008) Source characterization of the 6 August 2007 Crandall Canyon Mine seismic event in central Utah. Seismological Research Letters 79.5, 2008: 637-644.

Gale, W.J. (1999) Experience of field measurement and computer simulation methods of pillar design. In *Proceedings of the Second International Workshop on Coal Pillar Mechanics and Design. Vail, CO. 1999.* 49-61

Garvey, R. (2013) A study of unstable rock failures using finite difference and discrete element methods. Ph. D. Thesis, Colorado School of Mines, Golden, Colorado, USA.

Garvey, R. and Ozbay, U. (2012) Identifying unstable failure in brittle rock using the finite difference method. ARMA 12-422, Proceedings of the 46th U.S. Rock Mechanics/Geomechanics Symposium, Chicago, IL, June 24-27, 2012.

Garvey, R. and Ozbay, U. (2013) Assessing coal bumps from excess energy in finite difference models. Proceedings of the 32nd International Conference on Ground Control in Mining, Morgantown, WV, July 30, 2013.

Gates, R.A. et al. (2008) Report of investigation: underground coal mine, fatal underground coal burst accidents, August 6 and 16, 2007, Crandall Canyon mine, Genwal Resources, Inc., Huntington, Emery County, Utah, ID No. 42-01715. Arlington, VA: U.S. Department of Labor, Mine Safety and Health Administration.

Gu, R. (2013) *Distinct element model analyses of unstable failures in underground coal mines*. Ph. D. Thesis, Colorado School of Mines, Golden Colorado, USA.

Iannacchione, A.T. (1990). The effects of roof and floor interface slip on coal pillar behavior. Proceedings of the 31st US Symposium on Rock Mechanics.

Itasca Consulting Group Inc. (2013) FLAC3D (Fast Lagrangian Analysis of Continua in 3 Dimensions), Version 5.0. Minneapolis, MN.

Itasca Consulting Group Inc. (2013) UDEC (Universal Distinct Element Code) Manual, version 4.0. Minneapolis, MN:Itasca Consulting Group Inc; 2010.

Kias E, Garvey R, Gu R, Ozbay U. (2011). Modeling unstable rock failure during a uniaxial compressive strength test. 45th US Rock Mechanics/Geomechanics Symposium; 11-442:1-9.

Larson, M.K. and Whyatt, J.K. (2012) Load transfer distance calibration of a coal panel scale model: a case study. 31st International Conference on Ground Control in Mining.

Mark, C. (1990) Pillar design methods for longwall mining. Pittsburgh, PA: U.S. Department of the Interior, Bureau of Mines, IC 9247. NTIS No. PB 90-222449.

Mark, C. (1999) Pillar design methods for longwall mining. U.S. Dept. of the Interior, U.S. Bureau of Mines.

Mishra, B., & Nie, D. (2013). Experimental investigation of the effect of change in control modes on the post-failure behavior of coal and coal measures rock. *International Journal of Rock Mechanics and Mining Sciences*, *60*, 363-369.

Pariseau, W. (2011) Geomechanics of Crandall Canyon barrier pillar mining. SME Annual Meeting, Denver, CO, 2011.

Pechmann, J.C., et al. (1995) The February 3, 1995, ML 5.1 seismic event in the Trona mining district of southwestern Wyoming. Seismological Research Letters, 66(3), 25-34.

Pechmann, J.C., et al. (2008) "Seismological report on the 6 August 2007 Crandall Canyon mine collapse in Utah." *Seismological Research Letters* 79.5 (2008): 620-636.

Peng, S.S. and Chiang, H.S. (1984) Longwall mining. New York: Wiley and Sons.

Poeck, E., Zhang, K., Garvey, R. and Ozbay, M. (2015) Energy concepts in the analysis of unstable coal pillar failure. Proceedings of the 34th International Conference on Ground Control in Mining, Morgantown, WV, USA, July 28-30.

Rao, T. V. (1974) Two Dimensional Stability Evaluation of a Single Entry Longwall Mining System. M. S. Thesis, Department of Mining Engineering, University of Utah.

Ryder, JA. (1988) Excess shear stress in the assessment of geologically hazardous situations. JS Afr Inst Min Metall 1988;88(1):27-39.

Salamon M.D.G. and Munro, A.H. (1967) A study of the strength of coal pillars. J. S. Afr. Inst. Min. Metall. September.

Salamon, M.D.G. (1974) Rock Mechanics of Underground Excavations. Advances in rock Mechanics, Proc. 3rd Congr., Int. Soc. Rock Mech., Denver, 1B, 951-1099. Washington, DC: Nat. Acad. Sci.

Related literature

Abel, J. F. "Soft rock pillars." *Geotechnical and Geological Engineering* 6.3 (1988): 215-248.

Arabasz, Walter J., and James C. Pechmann. "Seismic characterization of coal-mining seismicity in Utah for CTBT monitoring." *Lawrence Livermore National Laboratory internal report UCRL-CR-143772* (2001).

Babcock, C.O., and D.L. Bickel. Constraint—the missing variable in the coal burst problem. In *Rock Mechanics in Productivity and Protection - Proceedings of the 25th Symposium on Rock Mechanics. Littleton, CO. Society for Mining, Metallurgy, and Exploration, Inc*.1984.

Badr, S. (2004) Numerical Analysis of Coal Yield Pillars at Deep Longwall Mines, PhD Dissertation, Colorado School of Mines.

Bieniawski, Z.T. (1967)An analysis of results from underground tests aimed at determining the *in situ* strength of coal pillars. CSIR Report MEG 569, Pretoria, South Africa, July, 1967; Rock Mechanics Division, National Mechanical Engineering Research Institute Council for Scientific and Industrial Research, Leipzig, 1967.

Bieniawski, Z.T. (1966) Stable and unstable fracture propagation in rock. Report of the South African Council of Scientific and Industrial Research No. MEG 493, October, 1966.

Bigoni, D. and Hueckel, T. (1991) Uniqueness and localization -I. Associative and non-associative elastoplasticity. International Journal of Solids and Structures. Vol. 28, No. 2, pp. 197-213, 1991.

Brady, B.H.G., and E.T. Brown (2006) "Energy, mine stability, mine seismicity and rockbursts." Rock Mechanics for underground mining (2006): 271-311.

Boni, P. and Atkinson Jr., W. "A Mineralogical, Stratigraphic, and Geochemical Profile of Trona Bed 17 in the Solvay Trona Mine near Green River, Wyoming." Proceedings of the 34th Forum on the Geology of Industrial Minerals, 1998.

Caldwell, J. (2009) SME on Crandall Canyon and mining bumps. http://ithinkmining.com/2009/02/25/sme-on-crandall-canyon-and-miningbumps/, Accessed on 2/20/2013.

Chase, F., Zipf, Jr., K. and Mark, C. (1994) The massive collapse of coal pillars - case histories from the United States. Proc. 13th International Conference on Ground Control in Mining, pp. 69-80.

Culbertson, William C. (1971) "Stratigraphy of the trona deposits in the Green River Formation, southwest Wyoming." *Rocky Mountain Geology.* 10.1 15-23.

Cundall, P. A., and J. V. Lemos. (1990) Numerical simulation of fault instabilities with a continuously-yielding joint model. *Rockbursts and Seismicity in Mines, Balkema, S*: 147-52.

Damjanac, B., M. Pierce, and M. Board. "Methodology for Stability Analysis of Large Room-and-Pillar Panels. " *48th US Rock Mechanics/Geomechanics Symposium*. American Rock Mechanics Association, 2014.

Esterhuizen, G. and Mark, C. (2009) Three-dimensional modeling of large arrays of pillars for coal mine design. Proceedings of the International Workshop on Numerical Modeling for Underground Mine Excavation Design, pp. 37-46.

Esterhuizen, G., Mark, C. and Murphy, M. (2010) The ground response curve, pillar loading and pillar failure in coal mines. 29th International Conference on Ground Control in Mining, pp. 19-27.

Esterhuizen, E., C. Mark, and M.M. Murphy. Numerical model calibration for simulating coal pillars, gob and overburden response. In *Proceeding of the 29th international conference on ground control in mining, Morgantown, WV*. 2010.

Ferriter, R.L., R.K. Zipf Jr, D.M. Ropchan, J. Davidson, (1996). Report of Technical Investigation, Underground Nonmetal Mine, Mine Collapse Accident, Solvay Mine, Solvay Minerals, Inc., Green River, Sweetwater County, Wyoming, Gebruary 3, 1995. Denver CO: U.S. Department of Labor, Mine Safety and Health Administration.

Goodspeed, T. and Skinner, J. (1996) Accident Investigation Report, Underground Nonmetal Mine, Fatal Collapse of Mine Workings Accident: Mine I.D. No. 48-01295, Solvay Minerals Inc. Mine, Solvay Minerals inc. Green River, Sweetwater County, Wyoming, February 3, 1995. U.S. Department of Labor, Mine Safety and Health Administration.

Gilbride, Leo J., and Michael P. Hardy. "Interpanel barriers for deep western US longwall mining." *Proceedings: 23rd International Conference on Ground Control in Mining*. Morgantown, WV, 2004.

Gu, R. (2013) *Distinct element model analyses of unstable failures in underground coal mines*. Ph. D. Thesis, Colorado School of Mines, Golden Colorado, USA.

Heasley, K. A. "LaModel analysis of the crandall canyon mine collapse." *Forty third US Rock Mechanics Symposium & 4th US–Canada Rock Mechanics Symposium, Asheville, North Carolina*. 2009.

Hill, R. (1958) A general theory of uniqueness and stability in elastic-plastic solids. Journal of the Mechanics and Physics of Solids, vol. 6, 1958, pp. 236-249.

Hustrulid, W.A. (1976) A review of coal pillar strength formulas. Rock Mechanics, Vol. 8, pp. 115-145.

Iannacchione, A.T. and Zelanko, J. (1995) Occurrence and remediation of coal mine bumps: a historical review. Proceedings of the Mechanics and Mitigation of Violent Failure in Coal and Hard-Rock Mines, vol. 01, pp. 27-68.

Iannacchione, A.T. and Tadolini, S.C. (2008) Coal mine burst prevention controls. 27th International Conference on Ground Control in Mining, pp. 20-28.

Kanamori, H., Mori, J., Hauksson, E., Heaton, T.H., Hutton, K., and Jones, L. M. (1993). Determination of earthquake energy release and ML using TERRAscope. *Bulletin of the Seismological Society of America* 83.2 330-346.

Kias E, Garvey R, Gu R, Ozbay U. (2011). Modeling unstable rock failure during a uniaxial compressive strength test. 45th US Rock Mechanics/Geomechanics Symposium; 11-442:1-9.

Koehler, J.R., DeMarco, M.J., and Wuest, W.J. (1995) The critical pillar concept in yield pillar-based longwall gate road design. SME Annual Meeting, March 6-9, 1995, Denver, CO.

Kripakov, N. and Kneisley, R. (1992) Pillar design in bump-prone deep westernU.S. coal mines. 11th International Conference on Ground Control in Mining,The University of Wollongong, N.S.W., pp. 72-83.

Lu, J., Ray, A., Morsey, K., and Peng, S. (2008) Effects of rock/coal interface property on coal pillar strength. 27th International Conference on Ground Control in Mining (ICGCM).

Lu, Z. and Wicks Jr, C. (2010) Characterizing 6 August 2007 Crandall Canyon mine collapse from ALOS PALSAR InSAR. Geomatics, Natural Hazards and Risk, 1(1), 85-93.

Maleki, Hamid, Kurt Hollberg, and Mike F. Jones. "A Fundamental Investigation of Pillar Foundation Failure in a Trona Mine." *48th US Rock Mechanics/Geomechanics Symposium*. American Rock Mechanics Association, 2014.

Mark, C. and Barton, T.M. (1996) The uniaxial compressive strength of coal: should it be used to design pillars? 15th International Conference on Ground Control in Mining, Golden, CO, August 13-15, 1996.

Mark, C. (2009) "Deep cover pillar recovery in the US." *Proceedings of the 28th International Conference on Ground Control in Mining*. 2009.

Mark, C. (2009) Deep cover pillar recovery in the US. 28th International Conference on Ground Control in Mining, Morgantown, WV, pp. 1-9.

Mark, C., and F.E. Chase. Analysis of retreat mining pillar stability (ARMPS). In *Proceedings-New Technology for Ground Control in Retreat Mining. Pittsburgh, PA: US Department of Health and Human Services, Public Health Service, Centers for Disease Control and Prevention, National Institute for Occupational Safety and Health, DHHS (NIOSH) Publication*. No. 97-122. 1997.

McGarr, A. (1994) A mechanism for high wall-rock velocities in rockbursts. Pure and Applied Geophysics, vol. 150, pp. 381-391.

Ng, L.K.W., Swan, G., and Board, M. (1993) The application of an energy approach in fault models for support design. Rockbursts and Siesmicity in Mines, pp. 387-391.

Ortlepp WD. The behaviour of tunnels at great depth under large static and dynamic pressures. Tunn Undergr Sp Tech 2001;16(1):41-8.

Ozbay, U. and Badr, S. (2010) Numerical modeling of yielding chain pillars in deep longwall coal mines. Workshop on Pillar Design. 29th International Conference on Ground Control in Mining, Morgantown, WV, 2010.

Oliver, J. and Huespe, A. (2007) Continuum approach to material failure in strong discontinuity settings. Computer Methods in Applied Mechanics and Engineering, vol. 193, no. 30, pp. 3195-3220, Jul. 2007.

Petukhov IM, Linkov AM. (1979) The theory of post-failure deformations and the problem of stability in rock mechanics. Int J Rock Mech Min Sci & Geomech Abstr 1979;16(2):57-76.

Plattner, C., et al. (2010) Surface subsidence induced by the Crandall Canyon Mine (Utah) collapse: InSAR observations and elasto-plastic modelling. Geophysical Journal International, 183(3), 1089-1096.

Poeck, E., Garvey, R., Zhang, K., and Ozbay, U. (2015) Contribution of shear slip in a widespread compressive pillar failure. The 49th US Rock Mechanics/ Geomechanics Symposium, San Francisco, CA, USA, 28 June-1 July, 2015Rabczuk, T. (2012) Computational methods for fracture in brittle and quasibrittle solids: state-of-the-art review and future perspectives. ISRN Applied Mathematics, eds. S. Li and R. Samtaney. Pre-publication, accepted September 3, 2012.

Richardson, Archie, J. F. T. Agapito, and Leo Gilbride. "Rock Mechanics Issues in the Trona Patch." *Proceedings of... International Conference on Ground Control in Mining*. Vol. 18. No. 1. Department of Mining Engineering, College of Mineral and Energy Resources, West Virginia University.

Salamon, M.D.G. (1984) Energy considerations in rock mechanics: fundamental results. JS Afr Inst Min Metall 1984;84(8):233-46.

Salamon, M. D. G. (1970) Stability, instability and design of pillar workings. Int J Rock Mech Min Sci & Geomech Abstr 1970;7(6):613-31.

Salamon, M., Badr, S. and Ozbay, M.U. (2003) Pillar failure in deep coal seams: numerical simulation. Technology Roadmap for Rock Mechanics, vol. 2, no. 10, pp. 1011-1018, Sep. 2003.

Shan, R., Jiang, Y. and Li, B. (2000) Obtaining dynamic complete stress-strain curves for rock using the Split Hopkinson Pressure Bar technique. International Journal of Rock Mechanics and Mining Sciences, vol. 37, pp. 983-992.

Shockey, D.A., Curran, D.R., Seaman, L., Rosenberg, J.T., and Petersen, C.F. (1974) Fragmentation of rock under dynamic loads. International Journal of Rock Mechanics and Mining Sciences & Geomechanics Abstracts, vol. 11, no. 8, August, 1974, pp. 303-317.

Swanson, P. L., and F. M. Boler. "The magnitude 5.3 seismic event and collapse of the Solvay trona mine: analysis of pillar/floor failure stability." *US Department of the Interior, Bureau of Mines, OFR* (1995): 86-95

Teaster, E.C. and Chao, E.L. (2008) Independent review of MSHA's actions at Crandall Canyon mine, Genwal Resources, Incorporated, Huntington, Emery County, Utah. US Department of Labor.

United States Mine Health and Safety Administration. (2008) Report of investigation, underground coal mine: fatal underground coal burst accidents, August 6 and 16, 2007, Crandall Canyon Mine, Genwall Resources Inc., Huntington Emergy County, Utah, ID, Issues 42-1715. Mine Safety and Health Administration, Office of the Adminstrator, Coal Mine Safety and Health, 2008.

U.S. Department of Labor (2007) Accidental Investigation Interview Transcripts and Exhibits for Genwal Resources Inc., Crandall Canyon Mine. Testimony of Al Davis, taken October 29, 2007, pp. 64-65. http://www.msha.gov/Genwal/transcripts/AI%20transcripts%20and%20exhibits/Al%20Davis%20Interview%20Transcript/1029AllynDavis.pdf. Accessed on 5/15/2015.

van Heerden, W.L. (1975) *In situ* complete stress-strain characteristics of large coal specimens. Journal of the South African Institute of Mining and Metallurgy, March 1975, pp. 207- 217.

Varley, F. and Whyatt, J. (2008) Work practices to manage bump prone ground. In Proceedings 27th International Conference on Ground Control in Mining (pp. 29-36).

Wagner, H. (1974) Determination of complete load deformation characteristics of coal pillars. Proceedings of 3rd ISRM Congress, Denver, CO, pp. 1076-1081.

Wang, L. et al. (2010) Controlling the effect of a distant extremely thick igneous rock in overlying strata on coal mine disasters. Mining Science and Technology, China, vol. 20, no. 4, pp. 510-515.

Whyatt, J. (2008) Dynamic Failure in Deep Coal: Recent Trends and a Path Forward. *Proceedings 27th International Conference on Ground Control in Mining*. 2008.

Whyatt, J.K. and Board, M.P. (1991) Numerical exploration of shear-fracture related rock bursts using a strain-softening constitutive model. RI 9350, United States Department of the Interior, Bureau of Mines, 1991.

Whyatt, J. and Loken, M. (2009) Coal Bumps and Odd Dynamic Phenomena-A Numerical Investigation. *28th International Conference on Ground Control in Mining*. 2009.

Whyatt, J. and Varley, F. "Catastrophic failures of underground evaporite mines." *Proceedings: 27th International Conference on Ground Control in Mining*. 2008.

Zhang, K., Poeck, E., Garvey, R., and Ozbay, M. (2015) Effect of coal-rock interface properties on failure stability of coal pillars expressed in energy terms. The 49th US Rock Mechanics/ Geomechanics Symposium, San Francisco, CA, USA, 28 June-1 July, 2015.

Zhao, J. (2000) Applicability of Mohr-Coulomb and Hoek-Brown strength criteria to the dynamic strength of brittle rock. International Journal of Rock Mechanics and Mining Sciences, vol. 37, pp. 1115-1121.

Zipf Jr, R. K. and Swanson, P. "Description of a large catastrophic failure in a southwestern Wyoming Trona Mine." *37th US Symposium on Rock Mechanics*. Vol. 1. Taylor & Francis US, 1999.

Zipf, R. Karl. "Toward pillar design to prevent collapse of room-and-pillar mines." *108th Annual Exhibit and Meeting, Society for Mining, Metallurgy and Exploration, Denver*. 2001.

Zipf Jr., R.K. and Mark, C. (1997) Design methods to control violent pillar failures in room-and-pillar mines. Transactions of the Institute of Mining and Metallurgy, vol. 106, pp. A124-A132.

Zou, D., Miller, H. and Kaiser, P. (1989) Numerical study of violent rock failure by stick-slip on joints. Mining Science and Technology, vol. 9, no. 3, pp. 241-251.

10. Appendices

APPENDIX I: Quasi-Static Calculation of Excess Energy

Energy Transfer during Mining

Stable failure occurs when the strength of the rock is exceeded and energy supplied from external sources is insufficient to further propagate failure. Stable failure is quasi-static and an ordinary consequence of progressive mining. In stark contrast is the phenomenon of unstable failure which is highly dynamic and emerges when more energy is released from a system than may be consumed through plastic deformations.

Cook likened unstable failures to a “soft” testing machine being used to fail a rock specimen in uniaxial compression (Cook, 1965; Salamon, 1970). This case is represented in Figure A1.1 in which the testing machine is idealized as a spring.

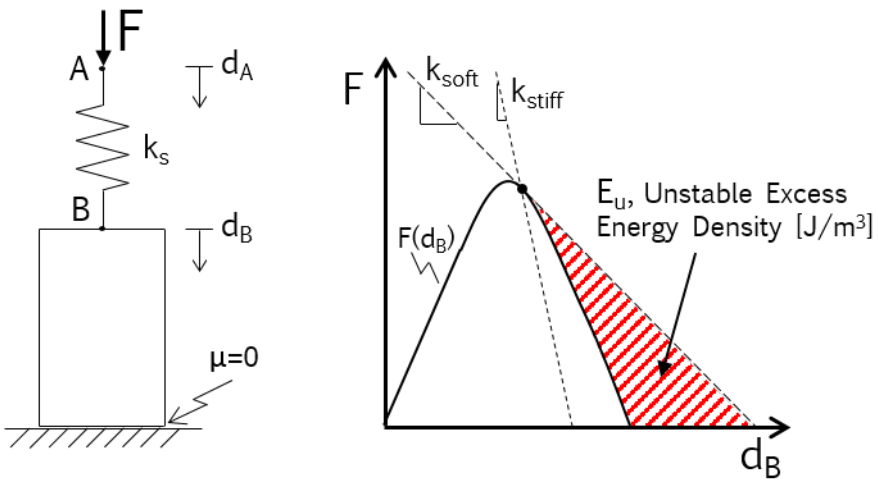

Figure A1. 1 Simple demonstration of unstable compressive failure

When a small displacement, d_a, is applied at point A, a force *F* is developed within the system and some energy is stored within the spring as elastic strain energy. As this application of displacements is continued, the force applied by the spring onto the rock specimen will eventually exceed the strength of the specimen. For a relatively stiff spring, a force-displacement equilibrium will be maintained between the spring and specimen throughout the failure which will only proceed through continued displacement at point A. For a sufficiently soft spring, the force applied by the spring will be greater than the specimen can resist and an unstable equilibrium emerges. Under these conditions of instability (state of being unstable), the specimen undergoes rapid failure as stored strain energy in the spring is released as kinetic energy into the system.

In the case of the stiff spring, all energy within the system may be accounted for using the quasi-static energy balance found in Equation 1. Boundary work, W_b, is first added through the displacements at point A. This boundary work is then stored as strain energy both within the spring, U_s, and within the specimen as U_c. When failure is initiated, plastic work, W_p, will be performed by the specimen. The sum of these terms accounts for stable and quasi-static compressive systems:

$$stable\text{: } W_b = U_s + U_c + W_p \qquad \text{(A1.1)}$$

During the emergence of unstable failure conditions, an additional term is needed to account for the excess energy released as kinetic energy during failure. This additional energy term will be referred to as unstable excess energy and may be found as the difference between the energy supplied to the system and the energy which is stored or absorbed through static processes. Equation A1.2 demonstrates this calculation of unstable excess energy which is equivalent to the kinetic energy released due to unstable equilibrium conditions emerging within the system.

$$unstable\text{: } E_u = W_b - \left(U_s + U_c + W_p\right) \quad \text{(A1.2)}$$

This same concept may be extended to the transfer of energy during the formation of underground excavations. A proposed energy balance has been developed to describe the transfer of energy during

mining which includes the potential for unstable excess energy to be released from unstably failing rock systems. The energy balance is shown as Equation A1.3 with associated energy notations listed in Table A1.1.

$$E_u = (W_b + W_t + W_i) - \left(U_c + W_p + U_j + W_j\right) \qquad \text{(A1.3)}$$

$$unstable\ failure\ if\ E_u > 0 \qquad \text{(A1.4)}$$

Table A1.1: Energy Components during Mining

W_b: External boundary work
W_t: Body work or the change in gravitational potential energy
W_i: Internal boundary work
U_c: Elastic strain energy in rock
W_p: Work done by plastic deformation of rock
U_j: Elastic strain energy stored along a joint
W_j: Frictional work performed along a joint
U_m: Elastic strain energy of mined material
E_u: Unstable excess energy

When the total energy in a geomechanical system may be accounted for through the static terms found in Equation A1.3, then the system may be considered stable. However, if some energy is not accounted for through the accumulation of static energy terms to the right of the equality, then the system may be thought of as unstable and the unstable excess energy takes a positive value.

The majority of the energy terms in Table A1.1 have historically been used to describe the quasi-static transfer of energy during mining (Cook, 1967; Salamon, 1984). One additional energy term, W_i, is introduced to describe the internal boundary work, or the work which is required to remove material from a stressed rock mass without the inherent release of kinetic energy. The term was developed to isolate the energy released due to instability from the energy released purely as a consequence of mining. This practice is useful in studies aimed at identifying unstable failure during progressive mining or tunneling sequences.

A1.2 Body Work and External Boundary Work

For the geomechanical system shown in Figure A1.2, energy may be supplied to the rock through gravitational loads and their resulting displacements (i.e. body work). In a simplified model of the system (shown to the right of the figure), energy may also be added through loads and displacements applied at the system's external boundaries such as the pressure boundary applied to the top of the system to represent the gravitational load of the overlying overburden.

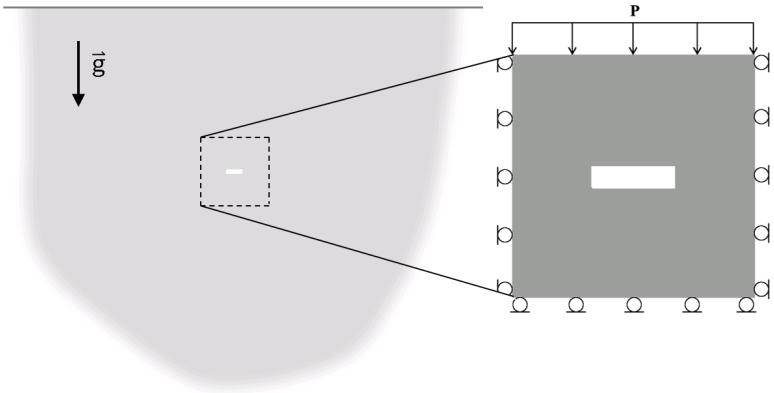

Figure A1.2: Rock mass loaded through boundary work

For a collection of gridpoints representing the distributed density of the rock mass in an explicit timestepping scheme, body work may be calculated in its standard form shown in Equation A1.5 where *N* is the total number of gridpoints in the system, *m* is the mass of each gridpoint, $\vec{g}$ is the gravitational acceleration, and $\vec{u}_n$ and $\vec{u}_{n-1}$ are the displacements from the current and previous steps, respectively.

$$W_t = \sum_{i=1,N}[m \cdot \vec{g} \cdot (\vec{u}_n - \vec{u}_{n-1})]_i \qquad \text{(A1.5)}$$

The external boundary work may be found from the summation of work terms across the system's loading surface. The boundary work for a given timestep is found from Equation A1.6, where N_b is the total number of points along the loaded boundary, $\vec{F}_n$ is the current applied force vector at a point while $\vec{F}_{n-1}$ is the force which was applied in the previous timestep.

$$W_b = \frac{1}{2}\sum_{i=1,N_b}\left[\left(\vec{F}_n + \vec{F}_{n-1}\right) \cdot (\vec{u}_n - \vec{u}_{n-1})\right]_i \qquad \text{(A1.6)}$$

A1.3 Internal Boundary Work during Progressive Mining Steps

As an excavation is formed stresses are removed along the newly formed free face. This removal of stress will result in a convergence of the surrounding rock mass into the excavated area and a subsequent release of energy. To account for continuously changing mine geometries, a method was developed to remove material from a continuum model in a quasi-static manner while accounting for the energy which is released through the deformation of the newly freed, internal boundary.

For the system shown in Figure A1.3 in which an existing excavation is enlarged by volume V_m, the newly formed surface S_m will deform until zero tractions remain along its length. When material has been removed, some stored energy will be released from the surrounding rock mass and the boundary of the newly enlarged excavation will deform until a static equilibrium is achieved. The dynamic response of

the rock mass in a physical mining case will be highly dependent upon the method used for removing material. If mechanical excavation is employed then the boundary around the excavation will deform in a slow and quasi-static process. However, if a sudden removal of material occurs, such as in the case of drill-and-blast operations, then much of the deformation of the internal boundary will occur suddenly and dynamically.

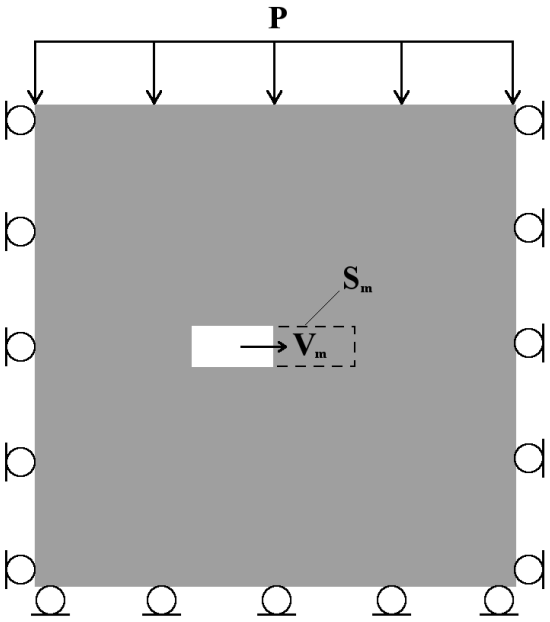

Figure A1.3: New excavation boundary, S_m

The deformation process of the internal boundary may take different forms. However, the precise details of the transition from the pre-mined to the mined state are not a necessary component for studying the energy which arises as a consequence of unstable equilibriums within the rock mass. A special control may be applied to numerical models to track the deformations of internal boundaries due to mining to bring the system to a new equilibrium state through a quasi-static process, rather than an inherently dynamic one. This is a simplification of the failure process which may ignore certain dynamic effects on the evolution of unstable failures, however the focus of this method is a quasi-static one which does not assume a realistic dynamic response for the selected failure criterion or time stepping scheme. The emergence of unstable failure conditions may then be studied within a changing mine geometry.

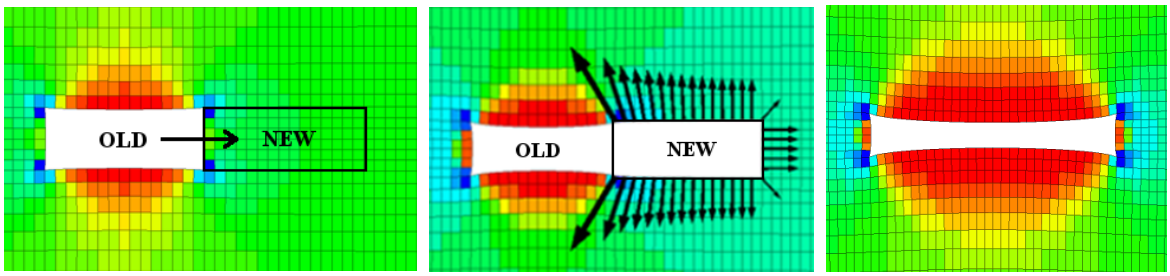

Figure A1.4: Demonstration of internal boundary control before, during, and after mining in FLAC^{3D}

A numerical procedure to control closures following mining steps is shown in Figure A1.4. The process involves first the removal of material which is to be mined. Forces are then applied onto the newly formed internal boundary which are equal to the pre-mining tractions. These forces are then gradually reduced while the resultant displacements are recorded along the boundary. In this manner it becomes possible to identify any excess energy which comes exclusively from unstable failures of brittle rock behind or around the active mining face when analyzing the effects of progressive mining. Table A1.2 lists these steps for applying internal boundary forces in FLAC^{3D}.

Table A1.2: Steps for Applying Internal Boundary Control after Excavating

1. Remove material from active excavation (Figure A1.4, left)
2. Apply forces along active excavation which are equal to the pre-mining tractions acting across the surface of the newly mined volume (Figure A1.4, middle)
3. Reduce forces along active excavation
4. Record internal boundary work after points have displaced
5. Repeat process starting at step 2 until the applied forces are reduced to zero (Figure A1.4, right)

By using this proposed procedure, it becomes possible to record the applied forces and resultant displacements which were required to deliver the rock mass to static equilibrium following the removal of mined material. Following a reduction of applied tractions, the increment of internal boundary work, ΔW_i, is then calculated in the same manner as the previous calculation of external boundary work. Equation A1.7 demonstrates this approach where N_i is the total number of points along the previously mined and the newly mined boundaries.

$$\Delta W_i = \frac{1}{2}\sum_{i=1,N_i}\left[\left(\vec{F}_n + \vec{F}_{n-1}\right)\cdot\left(\vec{u}_n - \vec{u}_{n-1}\right)\right]_i \qquad \text{(A1.7)}$$

Note that due to the opposing directions of applied forces and resultant displacements, the internal boundary work will always take negative values with energy being removed from the system through the internal boundary controls described in Table A1.2.

A1.4 Elastic Strain Energy and Plastic Work

Energy added to the system will be stored as elastic strain energy or consumed through plastic work once the strength limit of the rock is exceeded. The elastic strain energy of a closed system with volume V_t may be found by taking the volume integral of the strain energy density function as in Equation A1.8. These values of elastic strain energy may be found readily for purely elastic materials from the relation shown in Equation A1.9, where stresses and strains are given at a point in the system.

$$U_c = \int_{V_t} \phi \, dV \qquad \text{(A1.8)}$$

$$\phi = \frac{1}{2}\sigma_{ij}\varepsilon_{ij} \qquad \text{(A1.9)}$$

After some manipulation, the elastic strain energy may be found directly from stresses and elastic material properties. This is demonstrated in Equation A1.10 where principal stresses are used to calculate the strain energy density.

$$\phi = \frac{1}{2E}[\sigma_1^2 + \sigma_2^2 + \sigma_3^2 - 2\nu(\sigma_2\sigma_3 + \sigma_3\sigma_1 + \sigma_1\sigma_2)] \qquad \text{(A1.10)}$$

This calculation of strain energy may be extended to explicit numerical models if separable sub-volumes are used for determining stresses and strains. Equation A1.12 may then be used to calculate ΔU, or the change in elastic strain energy. The elastic strain energy may be found for the previous step (*n*-1) and for the current step, *n*, from Equation A1.11 with the total number of calculation zones being expressed as *M* and each zone having its own volume *V*.

$$U_n = \sum_{i=1,M} \frac{V_i}{2E}[\sigma_1^2 + \sigma_2^2 + \sigma_3^2 - 2\nu(\sigma_2\sigma_3 + \sigma_3\sigma_1 + \sigma_1\sigma_2)]_i \qquad \text{(A1.11)}$$

$$\Delta U = U_n - U_{n-1} \qquad \text{(A1.12)}$$

The total magnitude of energy required to move from one static state to another, ΔE, may be calculated for the total strain energy change of each zone. This approach is demonstrated in Equation A1.13 which uses Cauchy stress and strain tensors with ε_{ij} representing mechanical shear strain.

$$E_n = \sum_{i=1,M} \frac{V_i}{2}[\sigma_{11}\varepsilon_{11} + \sigma_{22}\varepsilon_{22} + \sigma_{33}\varepsilon_{33} + 2\sigma_{12}\varepsilon_{12} + 2\sigma_{23}\varepsilon_{23} + 2\sigma_{13}\varepsilon_{13}]_i \qquad \text{(A1.13)}$$

$$\Delta E = E_n - E_{n-1} \qquad \text{(A1.14)}$$

For a material capable of failure, the resulting increment of plastic work, ΔW_p, is then simply the difference between the total change in strain energy and the change in elastic strain energy over a given timestep (Itasca, 2010).

$$\Delta W_p = \Delta E - \Delta U \qquad \text{(A1.15)}$$

An energy term which is conspicuously missing from our derived energy balance is the elastic strain energy of the material removed from the system, U_m. Prior to mining, the elastic strain of the material is included within the energy balance as U_c while plastic strain is recorded as W_p. Following mining, the pre-mining elastic strain energy of the removed material, U_m, is simply not accounted for in the subsequent calculations of U_c because the mined material lies outside of the newly defined system boundary. Note, however, that the plastic work consumed by this volume of rock was performed prior to its removal and remains a component of the total plastic work in the system.

A1.5 Energy Discussion

Viewing the problem of rockbursts and coal bumps from an energy standpoint enables a straightforward assessment of the level of instability which is experienced within given mining conditions and changing mine geometries. Historical efforts which have focused on the energy released during the formation of an excavation have touched upon the energy concerns leading to potentially dangerous mining conditions, yet have most frequently assumed elastic material properties for the rock mass. Modern numerical methods which are capable of simulating brittle material response may be used to extend these energy concepts to study the emergence of unstable failure conditions as they evolve within a changing mine environment. The techniques outlined demonstrate how to effectively apply these methods to calculate the unstable excess energy which is released through unstable failure by reducing all other dynamic effects during simulated mining.

Quasi-brittle constitutive models may be applied to either the rock mass or to pre-existing faults in order to study the kinetic energy which is released during the failure of these features once they emerge within potentially complex mining geometries or sequences. The sum of the unstable excess energy is then equal to the kinetic energy generated at the source of the failure which is equal to the local magnitude of seismic energy, a value commonly calculated from seismic records of mine failures and fault slips.

When the proposed energy balance is applied to studies of unstable failure conditions, brittle constitutive material models must be assigned either within a volume of rock failing due to compression or along a fault which is undergoing sudden slip. Otherwise, no unstable equilibrium will arise and the released kinetic energy will remain a nominal value. Modern numerical methods prove capable of satisfying these requirements (Kias et al., 2011), yet continued efforts should be applied to develop material models which are more suited to capturing the dynamic effects seen in rockbursts and coal bumps.

Appendix II: Extended FLAC 3D Analysis

March 10 Bump:

The results of the Mohr-Coulomb strain-softening models indicated that some unstable failure conditions occurred during the development and retreat of the North barrier section. These failures remained localized expressions of unstable failure, affecting only individual pillar ribs. A demonstration of where this instability was recorded is shown as Figure A2.1. These figures display the zones experiencing the largest shear strain rate (Garvey and Ozbay, 2012) before development of the North Barrier section entries, during development, and then after retreat of the two southern-most pillars.

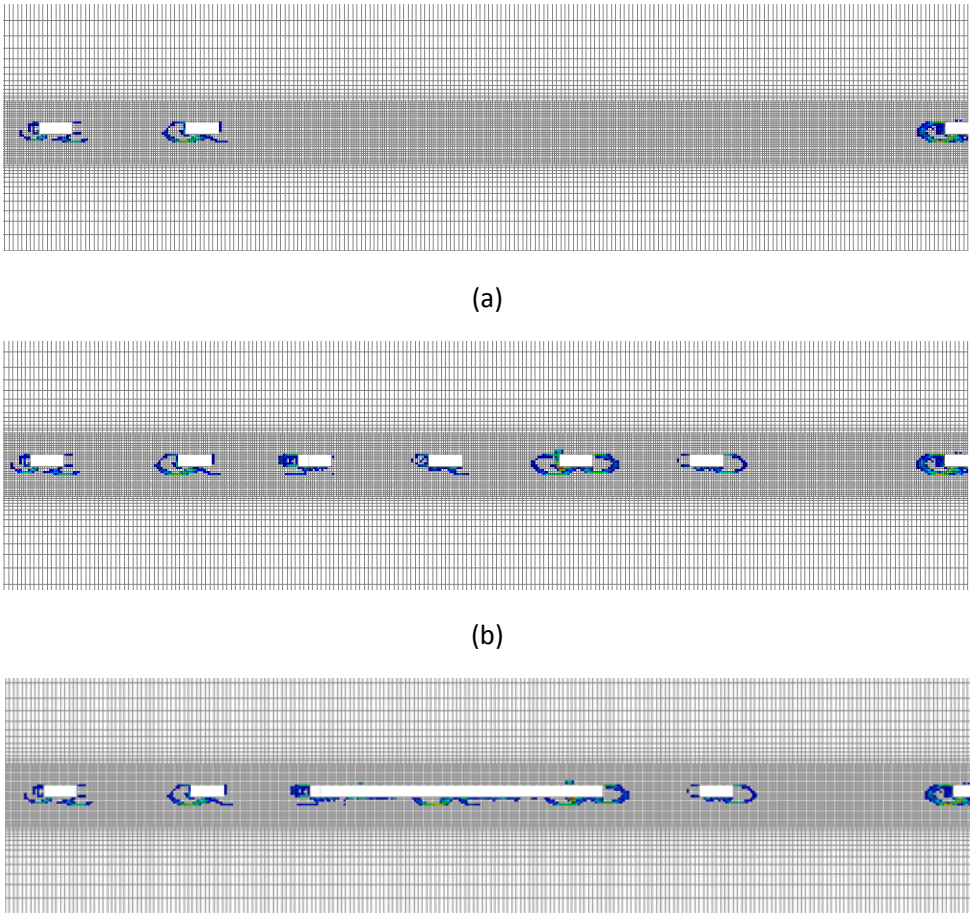

(a)

(b)

(c)

Figure A2.1 FLAC3D pillar damage shown by colored contours during simulated March 10 bump at the a) pre-mining, b) development, and c) retreat stage

The plots given in Figure A2.2 demonstrate the stress distribution for these same mining stages. The gray bars demonstrate the averaged stresses across each primary support structure. The red bars show the allowable stress of these structures if a 0.8 pillar stability factor (PStF) is assumed in conjunction

with the Mark-Bieniawski pillar strength formula given Equation A2.1. A 6.2 MPa cubic strength of coal and an infinite length in the third direction are assumed in this equation.

$$S_p = S_1 \left[0.64 + \left(0.54 \cdot \frac{w}{h}\right) - 0.18 \cdot \frac{w^2}{Lh}\right] \qquad \text{(A2.1)}$$

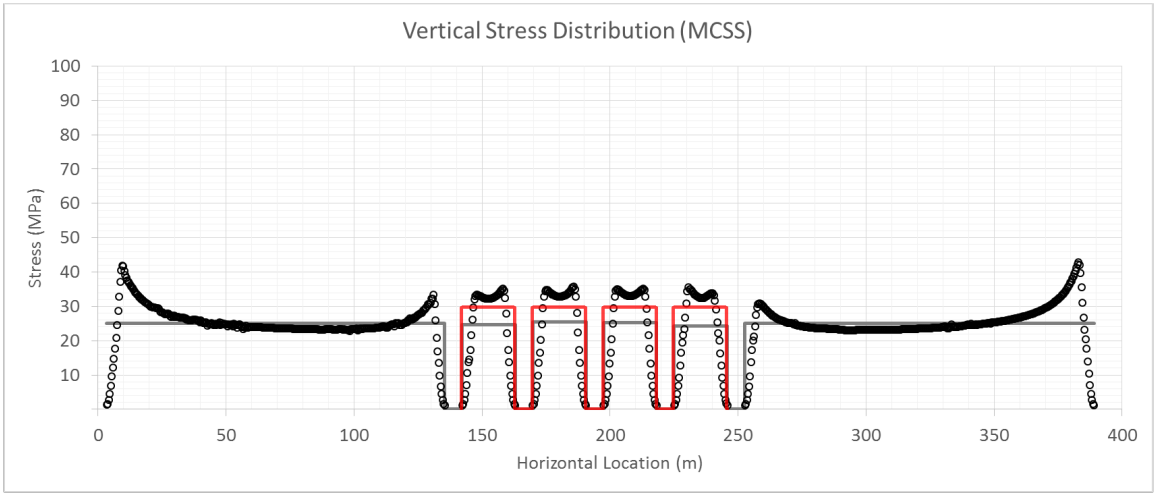

Figure A2.2 Profile of vertical stress along the top of the coal seam following Main West development and application of abutment loads. The gray bars show the average pillar stresses while red bars indicate allowable stresses.

No pillar stresses were seen to exceed the allowable stresses following the simulated development of the Main West entries or the application of side abutment loads. However, as the North Barrier pillar section was developed into smaller pillars (see Figure A2.3), some of these pillar stresses were seen to marginally exceed allowable stresses.

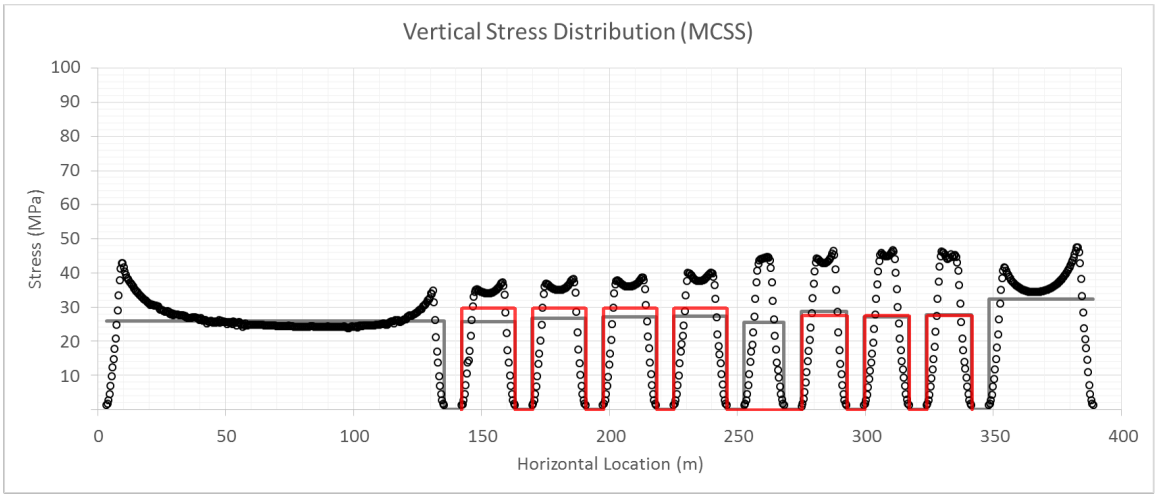

Figure A2.3. Profile of vertical stress along the top of the coal seam following development of North Barrier section. The gray bars show the average pillar stresses while red bars indicate allowable stresses.

After the retreat of the pillars in the North barrier section, pillar stresses far exceeded the load limits shown in Figure A2.4 due to the high abutment loads applied onto them from the neighboring longwall panels. The remaining pillar in the North Barrier section along with multiple pillars in the Main West section were seen to carry excessively high loads for their given dimensions.

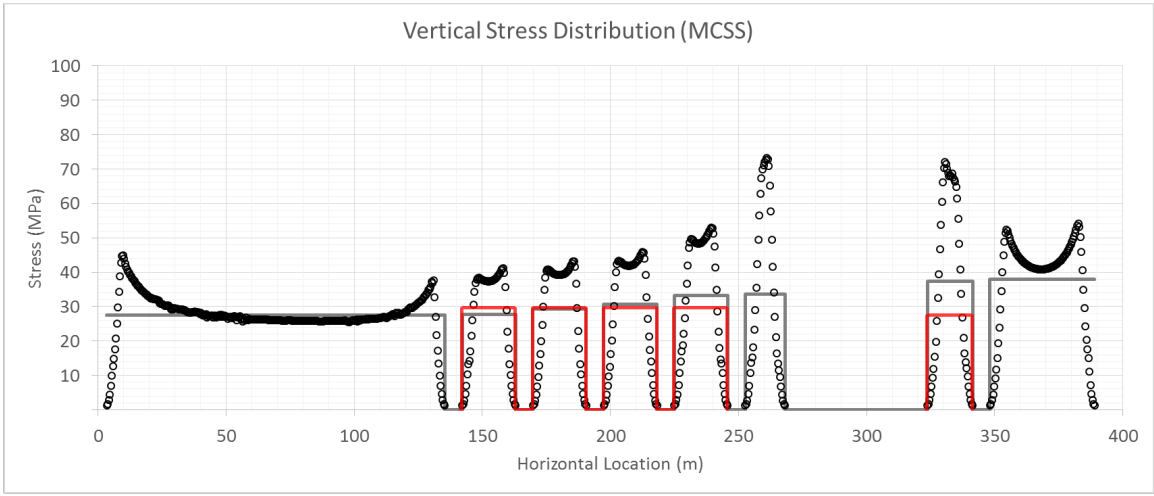

Figure . A2.4: Profile of vertical stress along the top of the coal seam following Main West development and application of abutment loads

The recorded magnitudes of excess energy during these periods of mining demonstrate a series of smaller unstable failure events, but the sizes of these failures remained relatively small and were localized within pillar ribs. The total unstable energy magnitudes are reported for the three different coal materials in terms of MJ per meter of extent in the third direction. Higher levels of excess energy were calculated in the case of the brittle MCSS material model. Significant numerical noise came into the calculation of the NB retreat due to dynamic oscillations of the large roof span during the removal of pillars in this section. These oscillations caused large magnitudes of erroneous energy release in the models. The development of a more controlled unloading procedure should be considered for future numerical models aimed at simulating pillar retreat.

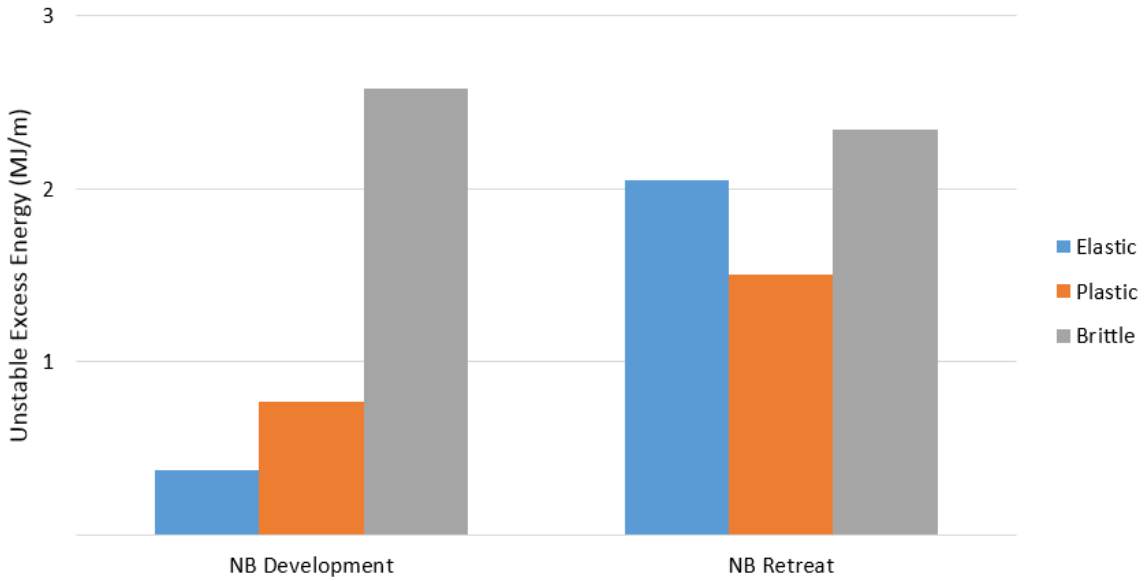

Figure A2.5. FLAC3D excess energy during development and pillar retreat in the North Barrier (NB) section

A noteworthy component of the March 10 bump event is the separation of several feet of coal from the overlying roof. This could be supportive of a slip failure along the coal-rock interface and promotes the possibility that the March 10 bump was indication of a more complex mode of pillar failure than pure compression. This aspect is considered in detail within the UDEC analysis involving the potential for shear slip along the coal-rock interface.

August 6 Bump

A primary component of the numerical analysis of the August 6th bump event was to assess how the massive collapse could be sustained in a panel with high width-to-height ratio pillars which maintained highly confined inner cores through their squat geometries. The remnant barrier was of a width of 120 feet in the area of collapse and, at the initial mining height of 2.4 m, maintained a width-to-height ratio of 15. Pillars of this width are typically thought to be hardening in a traditional compressive sense, with failure instead being observed as floor heave or due to the pillar punching into the roof or floor (Mark, 2000). However, in the Crandall Canyon collapse, these exceedingly large width-to-height ratio pillars were not only seen to fail but were seen to fail in a sudden and highly dynamic manner. The largest subsidence was measured directly over the remnant barrier pillar and a non-retreated area of pillars within the South Barrier section as seen in Figure 4.2. These trends indicate that the greatest failure occurred within this section and/or that the highest magnitudes of abutment stresses were redistributed onto these portions of the mine during the failure.

The August 6 collapse was initiated as retreat operations were being conducted in the South barrier section. This state corresponds to the transition of the mine geometry from the FLAC3D layout indicated in Figure 4 and that shown in Figure A2.6.

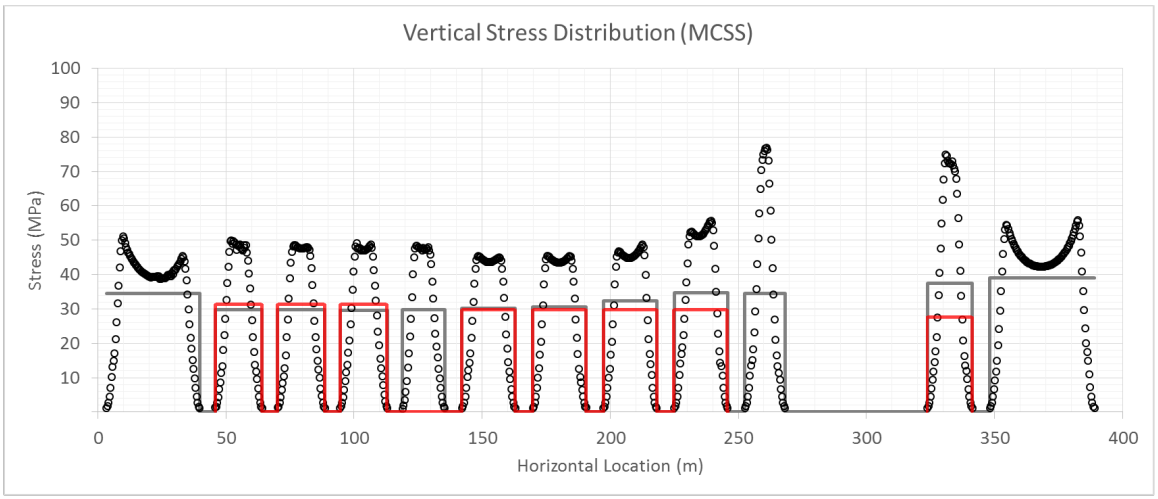

Figure A2.6. FLAC3D vertical stress distribution following development in South Barrier section

Even prior to retreat mining in the South Barrier section, the vertical stresses are seen to exceed allowable stress limits and the pillar strengths are seen to be insufficient to support the given loads at an assumed depth of 610 m. For a more conservative analysis this overburden height could be extended to its maximum of 660 m, yet the less conservative approach which was selected provides insight on the averaged behavior across the portion of the panel which was believed to have collapsed.

The subsidence at the top of the model was also recorded and is reported in Figure A2.7 following the development of the South barrier section. The FLAC3D subsidence values which were a result only of pillar development in the South Barrier section were seen to be significantly lower than those determined through the InSAR analysis following the collapse (shown as dashed line). The small magnitudes of vertical subsidence measured in the model does not reflect the direct observations following the collapse with the effect being that body work calculated through the static energy balance is much smaller than the change in gravitational potential energy in the physical collapse.

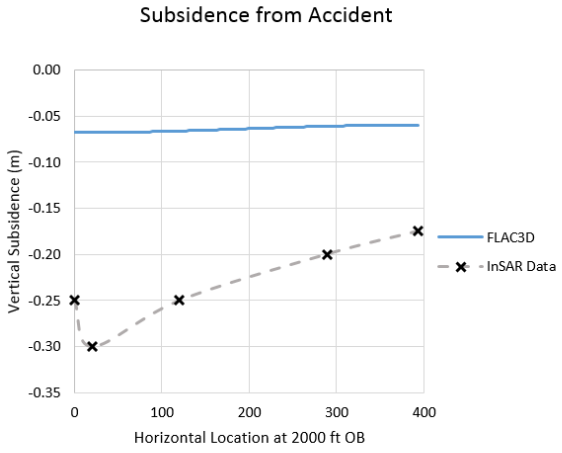

Figure A2.7. FLAC3D subsidence generated due to development of South Barrier section

The unstable excess energies which were calculated for the model following the development of the South barrier section are shown in Figure A2.8 for the three material models. The energy magnitudes calculated in the FLAC3D model only represent the energy which was released from a 0.4 m cross-section in the East-West direction of the mine. To extend these results across the length of the assumed collapse area, these energy terms were scaled across the 920 m of collapse length taken by Pechmann et al. (2008) in their seismic analysis. These magnitudes show that for the brittle Mohr-Coulomb strain-softening model indicated a collapse which released roughly 1.75 GJ in excess to the energy released when plastic or elastic material properties were assumed for the coal.

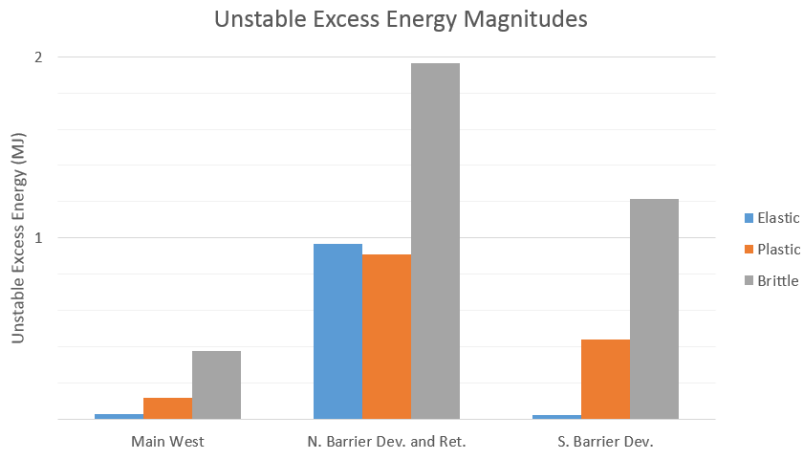

Figure A2.8: FLAC3D unstable excess energy magnitudes during mining stages

Ultimately, the lack of widespread pillar failure in the brittle coal models with a fixed pillar contact condition was found to be inconsistent with the massive failure observed in the August 6 collapse. Combined with an inability to model the subsidence contour following the accident, it was determined that a pillar with an infinite strength for the contact condition was unable to realistically simulate the extensive failure of the large width-to-height ratio pillars when a realistic compressive coal strength was applied to the seam. The full-scale analysis was therefore extended to a series of UDEC models which allowed for more extensive failure of the wide coal pillars by introducing potential shear failure of the coal-rock interface.

Appendix III: Input files for FLAC3D and UDEC models

See attached “Appendix III: FLAC3D and UDEC Input Files”

Appendix IV: Papers published from the project work

See the folder attached “Appendix IV: Published papers”

Disclaimer

This study was sponsored by the Alpha Foundation for the Improvement of Mine Safety and Health, Inc. (ALPHA FOUNDATION). The views, opinions and recommendations expressed herein are solely those of the authors and do not imply any endorsement by the ALPHA FOUNDATION, its Directors and staff.